

1 **Erk regulation of actin capping and bundling by Eps8 promotes cortex tension and leader bleb-**
2 **based migration**

3

4 Jeremy S. Logue^{1,2}, Alexander X. Cartagena-Rivera², Michelle A. Baird¹, Michael W. Davidson³, Richard
5 S. Chadwick² and Clare M. Waterman¹

6

7 ¹National Heart Lung and Blood Institute, National Institutes of Health, Bethesda, MD, 20892

8 ²National Institute on Deafness and other Communication Disorders, National Institutes of Health,
9 Bethesda, MD, 20892

10 ³National High Magnetic Field Laboratory and Department of Biological Science, The Florida State
11 University, Tallahassee, Florida, 32310

12

13 Corresponding authors: Clare M. Waterman (watermancm@nhlbi.nih.gov), Richard S. Chadwick
14 (chadwick@nidcd.nih.gov)

15 **Abstract**

16 Within the confines of tissues, cancer cells can use blebs to migrate. Eps8 is an actin bundling and
17 capping protein whose capping activity is inhibited by Erk, a key MAP kinase that is activated by
18 oncogenic signaling. We tested the hypothesis that Eps8 acts as an Erk effector to modulate actin
19 cortex mechanics and thereby mediate bleb-based migration of cancer cells. Cells confined in a non-
20 adhesive environment migrate in the direction of a very large “leader bleb.” Eps8 bundling activity
21 promotes cortex tension and intracellular pressure to drive leader bleb formation. Eps8 capping and
22 bundling activities act antagonistically to organize actin within leader blebs, and Erk mediates this effect.
23 An Erk biosensor reveals concentrated kinase activity within leader blebs. Bleb contents are trapped by
24 the narrow neck that separates the leader bleb from the cell body. Thus, Erk activity promotes actin
25 bundling by Eps8 to enhance cortex tension and drive the bleb-based migration of cancer cells under
26 non-adhesive confinement.

27 Introduction

28 Cell migration mediates critical physiological processes including development and the immune
29 response, and is de-regulated during cancer metastasis. Cells move by orchestrating their extracellular
30 interactions with intracellular cytoskeleton-dependent changes in shape and force generation; protruding
31 forward, grasping sites in the environment, and pulling themselves along (Lauffenburger and Horwitz,
32 1996; Papusheva and Heisenberg, 2010). Although the pulling forces driving cell movement are well
33 known to be mediated by myosin-based contraction (Vicente-Manzanares et al., 2009), recently it has
34 become clear that migrating cells can utilize multiple mechanisms to drive protrusion and interaction with
35 their environment (Lammermann and Sixt, 2009). Protrusion of the cell's plasma membrane boundary
36 can be driven by either actin polymerization or by pressure-driven membrane blebbing (Charras and
37 Paluch, 2008), while grasping the environment can be mediated by specific adhesion receptors that bind
38 to the extracellular matrix or other cells, or by non-specific friction (Bergert et al., 2015; Lammermann
39 and Sixt, 2009). These multiple modes of migration are adopted by different cells types in different
40 contexts. For example immune cells utilize adhesion-independent migration during tissue surveillance
41 (Lammermann et al., 2008), while endothelial cells utilize polymerization-driven protrusion during
42 angiogenesis (Lamallice et al., 2007).

43 Recent evidence indicates that physical confinement in a non-adhesive environment may drive a
44 change of migration modes. In particular, contractility and extracellular pressure can drive a switch from
45 polymerization/adhesion-based to bleb/friction-based motilities known as the mesenchymal-to-amoeboid
46 transition (MAT) (Bergert et al., 2015; Liu et al., 2015; Ruprecht et al., 2015). Cancer cells are known to
47 be highly contractile, making them prone to blebbing (Bergert et al., 2012), while tumors are known to be
48 sites of high turgor pressure (Jain, 1987), both properties being conducive to MAT. Indeed, intravital
49 imaging revealed that melanoma and breast cancer cells migrate by blebbing in live mice (Tozluoglu et
50 al., 2013). Thus, metastatic cancer cells are hypothesized to be susceptible to MAT *in vivo*, with the
51 plasticity of their migration modes and lack of specificity in adhesion contributing to their high invasivity
52 and difficulty targeting (Lammermann and Sixt, 2009).

53 Polymerization-driven mesenchymal migration and bleb-based amoeboid migration are
54 mechanistically distinct. In mesenchymal migration, actin polymerization initiated by localized activation
55 of a filament-nucleating factor drives the formation of actin networks or bundles that mediate
56 lamellipodial or filopodial membrane protrusion (Waterman and Skau, 2015). In contrast, in blebbing
57 cells, membrane protrusion is mediated by myosin II contractility-induced hydrostatic pressure that
58 drives a bubbling-out of the plasma membrane at a site of local weakness in the cortical actin
59 cytoskeleton (Charras and Paluch, 2008; Charras et al., 2005). While the molecular mechanisms
60 mediating polymerization-based protrusion and contractility-induced pressure are reasonably well
61 understood, the molecules responsible for local changes in the actin cortex that allow bleb formation are
62 not known. It is hypothesized that blebs could form either by local down-regulation of membrane-
63 cytoskeleton linkers such as those of the ezrin/radixin/moesin family (Estecha et al., 2009; Lorentzen et
64 al., 2011), or by local weakening of sites in the cortical actin network itself (Charras et al., 2006).
65 Indeed, experiments using actin depolymerizing drugs have shown cortex integrity to be an important
66 factor in regulating blebbing (Charras et al., 2006). Local inhomogeneity in cortical integrity could be
67 mediated by regulation of actin filament number or organization. In turn, filament number could be
68 controlled by modulating the activity of filament nucleators, cappers or depolymerizers, while actin

organization could be regulated by filament crosslinkers, bundlers or motor proteins. However, the proteins critical to regulating actin cortical organization and mechanics during blebbing are not known.

In this study, we focused on identifying the mechanism for regulating the actin cortex of cancer cells during MAT and bleb-based migration. Many highly invasive cancers are known to be caused by mutations that activate the oncogenic EGF/Ras/Raf/MEK/Erk pathway (Downward, 2003; Roberts and Der, 2007). It is well-known that Erk-mediated activation of myosin II promotes cell contractility (Klemke et al., 1997). Accordingly, we concentrated on actin regulatory proteins downstream of this pathway that may synergize with contractility to affect blebbing. Epidermal growth factor receptor pathway substrate 8 (Eps8) is an actin bundling and capping protein (Disanza et al., 2004; Disanza et al., 2006; Hertzog et al., 2010) that plays a critical role in development of the nervous, auditory and reproductive systems (Lie et al., 2009; Manor et al., 2011; Menna et al., 2009; Menna et al., 2013) and its upregulation in cancers correlates with invasivity and poor prognosis (Griffith et al., 2006; Kang et al., 2012; Wang et al., 2009). Eps8 was originally identified as an actin binding protein downstream of the EGF receptor and to regulate actin through a complex with SOS1 and Abi1 (Fazioli et al., 1993; Scita et al., 1999). Additionally, the actin filament capping activity of Eps8 is inhibited by Erk through phosphorylation (Menna et al., 2009). Thus, the dual actin regulatory functions and targeting by Erk make Eps8 a good candidate for regulating the cortex downstream of oncogenic signaling.

By combining imaging of fluorescently tagged proteins and atomic force microscopy (AFM) with targeted mutations in Eps8, the work described here tests the hypothesis that Eps8 acts as a key effector of Erk to modulate actin cortex mechanics and thereby mediate bleb-based migration of cancer cells. We find that Eps8 bundling activity promotes cortex tension and pressure to drive MAT in non-adherent, confined cells, which migrate with a characteristic “leader-bleb” morphology. Within leader blebs, Eps8 capping and bundling activities act antagonistically, and phosphorylation by Erk mediates this effect. Using a FRET biosensor for Erk, we document a massive concentration of kinase activity within leader blebs and find that leader bleb contents are trapped by the bleb neck that separates the bleb from the cell body. Our results identify a mechanism by which Eps8 may promote the transition to rapid, unregulated migration of cancer cells in confinement that may be critical to their highly invasive behavior *in vivo*.

97 RESULTS

98 Eps8 is recruited early to bleb membranes and forms a gradient across the length of a “leader 99 bleb”

100 To determine the role of Eps8 in cancer cell blebbing and migration, we utilized human A375
101 melanoma cells which carry a mutation in B-Raf (V600E) that activates the Raf/MEK/Erk pathway
102 (Davies et al., 2002). We imaged Eps8 and the actin cytoskeleton by spinning disk confocal microscopy
103 in cells that were fixed and stained with fluorescent phalloidin and either immunolabeled with antibodies
104 to Eps8 or expressing Emerald-tagged mouse Eps8 (GFP-mEps8). When cells were plated on
105 fibronectin-coated coverslips to promote adhesion and spreading, actin formed a dense meshwork in the
106 lamellipodia near the cell edge, and circumferential arcs and stress fibers in the lamella and cell body
107 (Figure. 1A). Both endogenous and Emerald-mEps8 localized primarily to lamellipodia and arcs, but
108 were absent from stress fibers (Figure. 1A, Figure 1-figure supplement 1A). To determine Eps8
109 distribution in a non-adhesive environment, A375 cells co-expressing Emerald-mEps8 and FusionRed-
110 tagged F-tractin (an actin filament binding peptide, (Schell et al., 2001)) were plated on uncoated glass.
111 Here, cells were rounded, and confocal sections midway through the cell Z-axis revealed a dense band
112 of cortical actin at the periphery of the cell body. From this cortical band extended many blebs that
113 possessed thin, continuous rims of cortical actin at their membranes (Figure. 1D). Eps8 was absent
114 from the dense cortical band of the cell body, but localized with actin in punctae along the peripheral rim
115 of actin in blebs (Figure. 1B, D). Co-expression of FusionRed-F-tractin and EGFP-tagged myosin II
116 regulatory light chain (GFP-MII-RLC, a marker of myosin II isoforms) in non-adherent cells showed that
117 myosin II was concentrated on the dense cortical band and was at very low levels or absent from the
118 bleb periphery (Figure. 1F). Thus, Eps8 shows differential localization to actin structures in adherent
119 spread and non-adherent blebbing melanoma cells.

120 We next sought to determine the dynamics of Eps8 in blebbing cells. Previous studies have
121 shown that shortly after bleb protrusion, the membrane-cytoskeleton linker protein ezrin is recruited to
122 the bleb membrane, followed by the assembly of actin, then myosin II, which induces bleb retraction
123 (Charras et al., 2006). To determine the timing of Eps8 arrival at the bleb membrane relative to these
124 proteins, we subjected A375 cells expressing EGFP tagged mEps8, ezrin, F-tractin, or MII-RLC to time-
125 lapse confocal imaging at 5 sec intervals. To mark the position of the cell membrane in negative-image,
126 cells were mounted in media containing red fluorescent dextran (Figure. 1C, E, G, Figure 1-figure
127 supplement 1B). Analysis of time-lapse image series showed that similar to previous studies, ezrin
128 appeared rapidly on the newly protruded bleb membrane at ~5 sec after bleb formation (Figures 1H,
129 Figure 1-figure supplement 1B). Recruitment of Eps8 and actin to the membrane occurred on a similar
130 timescale as ezrin (Figure. 1C, E, H). In contrast, MII-RLC appeared at ~30 sec after protrusion, and
131 coincided with the onset of bleb retraction (Figure. 1G, H). These results indicate that in non-adherent
132 cells, Eps8 recruitment to bleb membranes occurs concurrently with actin assembly.

133 To induce migration of non-adherent melanoma cells, we confined A375 cells expressing
134 Emerald-mEps8 and FusionRed-F-tractin between an agarose pad and uncoated glass (Bergert et al.,
135 2012). Strikingly, cells in these conditions had reduced blebbing on the cell body, but formed a single
136 very large sausage-shaped bleb that generally excluded the nucleus, and which was defined by a thin
137 neck at the junction between the large bleb and the spherical cell body (Figure. 1I & Video 1). This

morphology was very similar to the “A2” or “stable bleb” phenotypes recently described for non-adherent cells migrating under confinement (Bergert et al., 2015; Liu et al., 2015; Ruprecht et al., 2015). Long-term imaging showed that ~40% of non-adherent, confined cells exhibited apparently rapid migration in the direction of the very large bleb, which we will thus call a “leader bleb” (Video 2). Indeed, A375 cells adhered to fibronectin-coated coverslips (either 5 or 50 $\mu\text{g/ml}$) did not migrate, while leader bleb-based migration of confined non-adherent cells was very fast at $1.15 \pm 1.02 \mu\text{m/min}$ (mean \pm SE, Figure 1N).

Confocal imaging revealed that both Eps8 and F-actin were concentrated within the leader bleb relative to the cell body (Figure 1J, Figure 1-figure supplement 1C, Figure 1-figure supplement 2). To analyze the spatial distribution of actin and Eps8 within the leader bleb, we determined their average intensities within five regions of interest (ROIs), each representing 20% of the length of the leader bleb from neck (region 1) to distal tip (region 5) (Figure 1K). This showed that actin was distributed as circumferential bundles around the short axis of most of the length of the leader bleb, but was reduced at the bleb tip (Figure 1I, J, Figure 1-figure supplement 1C, Figure 1-figure supplement 2). Eps8 localized in a punctate manner along actin bundles, forming a gradient, with the highest concentration near the neck connecting the bleb to the cell body and the lowest level at the distal tip of the leader bleb (Figures 1K, Figure 1-figure supplement 1D, Figure 1-figure supplement 2). Time-lapse imaging and kymograph analyses showed that Eps8 and F-actin underwent coordinated retrograde movement from the distal leader bleb tip towards the bleb neck (Figure 1M & Video 3). Similar imaging of EGFP-MII-RLC showed that myosin II was distributed around the cortical band of the cell body, highly concentrated in the narrow neck at the bleb base where the bleb connected to the cell body, and nearly absent from the distal half of the leader bleb, similar to previous reports (Figure 1L)(Bergert et al., 2015; Liu et al., 2015; Ruprecht et al., 2015). Together, these results show that in non-adherent cells, Eps8 localizes rapidly to bleb membranes as actin assembles. When non-adherent cells are confined, actin and Eps8 concentrate in leader blebs where they exhibit a directional assembly gradient and rearward flow towards the contractile bleb neck, and this cortical flow is coordinated with rapid cell movement directed by the leader bleb.

Eps8 promotes leader bleb-based migration in cancer cells by maintaining actin bundles towards the distal bleb tip

We next sought to determine the requirement for Eps8 in the promotion of leader bleb-based migration and organization of the cortical cytoskeleton in confined, non-adherent cells. To test this, we used a small interfering RNA (siRNA) targeted to human Eps8 that resulted in $76 \pm 2.1\%$ (mean \pm SE) depletion of the protein in A375 cells after 24 hrs (Eps8-KD, Figure 2A). Expression of FusionRed-F-tractin in non-adherent Eps8-KD cells confined under an agar pad followed by confocal imaging revealed that Eps8 depletion generally inhibited the formation of large leader blebs (Figure 2B). Instead, confined non-adherent cells resembled unconfined non-adherent cells, with a distribution of various-sized protruding and retracting blebs around their perimeter (Figure 2B), and the fraction of cells that underwent leader bleb-based migration was reduced by nearly half (Figure 2D). To quantify the effects of Eps8-KD on bleb size, we used a simple definition of a leader bleb as the single largest bleb made by the cell, expressed as a percent of cell body area. This showed that Eps8-KD decreased leader bleb area by nearly half compared to non-targeting siRNA (Figure 2C & Supplementary File 1A). Expression of Emerald-mEps8 fully rescued leader bleb size and migration in Eps8-KD cells (Figures

2C-D, Figure 2-figure supplement 1C, Supplementary File 1A). Thus, Eps8 promotes formation of a large leader bleb to drive migration of confined, non-adherent A375 cells.

We then sought to determine whether the requirement for Eps8 in leader bleb-based migration was a more general property of cancer cells or specific to A375 cells. We tested this in U2OS human osteosarcoma that are deleted for the cell cycle regulatory gene CDKN2A (Catalogue of somatic mutations in cancer), and human lung cancer A549 cells that carry the K-Ras G12S oncogenic mutation (Catalogue of somatic mutations in cancer). When plated on uncoated glass, both U2OS and A549 cells rounded up and exhibited blebbing around their peripheries (Figure 2-figure supplement 2). When transfected with EGFP as a soluble marker and confined between uncoated glass and agar and subjected to time-lapse confocal microscopy, 36% of U2OS cells and 46% of A549 cells took on a leader bleb morphology (Figure 2-figure supplement 2) and underwent rapid migration (Figure. 2D). To test the requirement for Eps8 in this transition, we used siRNA to reduce Eps8 level by 53% and 57% in U2OS and A549 cells, respectively (Figure. 2A). Analysis of confocal movies showed that Eps8 depletion generally inhibited the formation of large leader blebs (Figure 2-figure supplement 2), and quantitation confirmed that the fraction of both cell types that underwent leader bleb-based migration was reduced by more than half, and leader bleb area was reduced by 34% and 43% in U2OS and A549 cells, respectively (Figure. 2C, D). Expression of Emerald-mEps8 rescued leader bleb size and migration in U2OS and A549 cells that had been treated with Eps8 siRNA (Figures 2C-D, Figure 2-figure supplement 2, Supplementary File 1A). Thus, Eps8 is required for leader bleb formation to drive migration of confined, non-adherent cells in several cancer cell types, independent of the oncogene driving transformation.

To analyze the effects of Eps8-KD on cytoskeletal organization (Figure. 2E-H), we utilized metrics that quantified both the density and bundle organization of the cytoskeleton in confined, non-adherent cells. For filament density, we measured average F-actin intensity in both the dense cortical actin band of the cell body and in the leader bleb (Figure. 2G, H). To quantify bundle organization, we determined the local alignment (“anisotropy”) of F-actin bundles within the leader bleb via the ImageJ plugin, FibrilTool, which uses the concept of nematic tensor to provide a local quantitative description of the anisotropy of fiber arrays and their average orientation in cells (Boudaoud et al., 2014) (Figure. 2H). To quantify the spatial variation in these parameters, we determined their values in five ROIs along the leader bleb length (Figure. 2H). This showed that compared to control, Eps8-KD induced a slight but significant reduction in the density of the cortical actin band in the cell body (Figure. 2E, G), but had no significant effect on the density or distribution of actin within leader blebs, where actin exhibited a gradient with the highest concentration at the neck (Figure. 2E, H). Regional analysis of F-actin anisotropy showed that in control cells, actin bundle alignment also formed a gradient in the leader bleb, but in the opposite direction as the density gradient, such that bundles consistently were most highly aligned towards the distal regions (Figure. 2H’), and decreased towards the neck. Knockdown of Eps8 did not destroy the anisotropy gradient, but made actin bundle organization highly variable along the largest bleb (Figure. 2H’). Examination of the localization of EGFP-MII-RLC in Eps8-KD cells showed that similar to control, myosin II concentrated in the dense cortical band of actin around the cell body and at the neck of the largest bleb (Figures 2F, Figure 2-figure supplement 1B). In agreement, western blotting for myosin II regulatory light chain phosphorylated on serine 19 (pS19 MLC) as a marker of activated myosin II showed no significant difference in myosin II activity between control and Eps8-KD (Figure. 2I). Together, these results show that in confined, non-adherent cells, Eps8 promotes

223 enlargement of leader blebs independent of myosin II activity, where it acts to promote actin bundling
224 towards the distal bleb tip, and is required for leader bleb-based migration.

225 **Cortex tension and intracellular pressure are maintained by Eps8**

226 Since leader bleb formation is mediated by intracellular pressure induced by contractility in the
227 cytoskeleton (Bergert et al., 2015; Liu et al., 2015; Ruprecht et al., 2015), we next sought to determine
228 the role of Eps8 in regulation of cortical cytoskeleton mechanical properties. We utilized an atomic force
229 microscope (AFM)-based assay in which rounded, non-adherent cells are subjected to a minimal
230 deformation with a tipless cantilever (Figure. 3A, B) (Fischer-Friedrich et al., 2014; Ramanathan et al.,
231 2015), and cortex tension and intracellular pressure can be extracted from the resulting force-
232 displacement curves using measurements of the cell radius and actin cortex thickness (Clark et al.,
233 2013) and a theory derived from a simple force balance of the applied cantilever normal force with the
234 force due to intracellular pressure and the force from cortex tension (see Methods). We first validated
235 the approach using cells treated with the myosin II ATPase inhibitor blebbistatin. This showed that
236 inhibition of myosin II did not significantly affect cell radius or cortical actin thickness, but cortex tension
237 and intracellular pressure were both significantly reduced (Figure. 3C-D, Figure 3-figure supplement 1,
238 Supplementary File 1), consistent with previous reports (Tinevez et al., 2009). Similar measurements
239 showed that compared to non-targeting control, Eps8-KD resulted in significant decreases in cortex
240 tension and intracellular pressure, although these effects were not as strong as those induced by
241 blebbistatin (Figure. 3C-D, Figure 3-figure supplement 1, Supplementary File 1). The effects of Eps8-
242 KD on mechanical properties could be rescued by re-expression of Emerald-mEps8 (Figure. 3C-D,
243 Figure 3-figure supplement 1, Supplementary File 1). Thus, Eps8 promotes cortex tension and
244 increases intracellular pressure. Together with our above results, this suggests that Eps8 regulates
245 cortical cytoskeletal organization to enhance cortical tension and increase intracellular pressure to
246 mediate leader bleb-based migration.

247 **Actin bundling by Eps8 promotes cortex tension and intracellular pressure to drive leader bleb**
248 **formation**

249 We next sought to test whether the actin bundling activity of Eps8 is required for leader bleb
250 formation and migration, cytoskeletal organization, and cellular mechanical properties. To accomplish
251 this, we made alanine substitutions within the C-terminus of Emerald-tagged mouse Eps8
252 (L757A/K759A, referred to as Emerald-mEps8 Δ bund, Figure. 4A) which have been previously shown to
253 specifically block Eps8 bundling activity (Hertzog et al., 2010). We co-expressed this together with
254 FusionRed-F-tractin or FusionRed-MII-RLC in either wild type or Eps8-KD cells in a non-adherent,
255 confined environment. This showed that Emerald-mEps8 Δ bund co-localized with actin at the thin
256 cortical rim on bleb membranes, similar to wild type Eps8 (Figures 4B, F, Figure 4-figure supplement 1).
257 However, in confined Eps8-KD cells, expression of Emerald-mEps8 Δ bund failed to rescue the defect in
258 leader bleb size induced by loss of Eps8, and these cells remained round and exhibited small blebs
259 around their periphery with no dominant leader bleb (Figures 4B-C, Figure 4-figure supplement 1,
260 Supplementary File 1A & Video 4). Accordingly, Eps8-KD cells expressing Emerald-mEps8 Δ bund
261 exhibited a more than 50% decrease in the fraction of cells migrating under confinement compared to
262 Eps8-KD cells reconstituted with Emerald-mEps8 (Figure. 4E). Even stronger effects on leader bleb
263 size were observed in wild-type A375 cells over-expressing Emerald-mEps8 Δ bund (Figure. 4D &

Supplementary File 1B), indicating it acts as a dominant negative, likely by dimerizing with endogenous Eps8 (Kishan et al., 1997). We thus used a dominant negative approach where appropriate to negate the possibility of off-target effects induced by siRNAs. Because cells carrying defects in Eps8 bundling activity lacked a large bleb, we were unable to determine the effects of this mutation on actin density or anisotropy in the leader bleb. However, analysis of actin density in the cortical band of the cell body showed that over-expression of Emerald-mEps8 Δ bund had no effect compared to over-expression of Emerald-mEps8 alone, and caused no detectable changes in the organization of MII-RLC (Figures 4F, Figure 4-figure supplement 1). AFM analysis showed that while over-expression of Emerald-mEps8 had no effect on cortical tension and intracellular pressure (Figure. 4H-I & Supplementary File 1), over-expression of Emerald-mEps8 Δ bund significantly reduced cortex tension and intracellular pressure compared to untreated controls (Figure. 4H-I & Supplementary File 1). These results show that the actin bundling activity of Eps8 facilitates the formation of large leader blebs by promoting cortical tension and intracellular pressure.

To further test the notion that F-actin bundling is critical to leader bleb formation and cell mechanical properties, we sought to determine if expression of a different actin bundling protein affected leader blebs or could rescue the defect in leader bleb size induced by loss of Eps8. We over-expressed the actin bundling protein α -actinin (Podlubnaya et al., 1975) tagged with EGFP together with FusionRed-F-tractin in either WT or Eps8-KD cells under non-adherent confinement. Confocal imaging of EGFP- α -actinin in either WT or Eps8-KD cells showed a remarkably similar localization as Emerald-mEps8 (Figure. 1I, Figure 1-figure supplements 1 & 2), with α -actinin concentrated in leader blebs where it was localized in a gradient along circumferential actin bundles, although the labelling of the bundles was more continuous and less punctate than that of Emerald-mEps8 (Figure 4-figure supplement 2). Quantitative analysis showed that in Eps8-KD cells, over-expression of α -actinin was sufficient to partially rescue their defect in leader bleb size, but not to the same extent as expression of Emerald-mEps8 Δ bund (Figure. 4C-D & Supplementary File 1). In addition, α -actinin over-expression in Eps8-KD cells partially rescued the effects of loss of Eps8 in cell migration (Figure. 4E). AFM analysis showed that over-expression of α -actinin increased cortical tension and intracellular pressure by more than 50% compared to either untreated cells or cells over-expressing Emerald-mEps8 (Figure. 4H-I & Supplementary File 1). These results demonstrate the critical role of actin bundling in promoting cortical tension and generating intracellular pressure to mediate the formation of leader blebs, however they show that other functions or regulation of Eps8 cannot be compensated by α -actinin.

Eps8 actin capping activity limits leader bleb size by decreasing actin density and mechanical properties in the cell body cortex, and antagonizing actin bundling at the leader bleb tip

We next sought to determine whether the actin filament capping activity of Eps8 is required for leader bleb formation, cytoskeletal organization, and cellular mechanical properties. We made aspartic acid substitutions within the C-terminus of Emerald-tagged mouse Eps8 (V689D/L693D, referred to as Emerald-mEps8 Δ cap) which have been previously shown to specifically block Eps8 capping activity (Figure. 4A) (Hertzog et al., 2010) and regulate blebbing during cell division (Werner et al., 2013). Strikingly, when RLCconfined under agar, Eps8-KD cells expressing Emerald-mEps8 Δ cap formed significantly larger leader blebs and the proportion of cells migrating nearly doubled compared to either untransfected controls or to Eps8-KD cells expressing Emerald-mEps8 (Figure. 5A, B, D,

Supplementary File 1 & Video 5). Over-expression of Emerald-mEps8 Δ cap similarly increased leader bleb area compared to over-expression of Emerald-mEps8 (Figure. 5C & Supplementary File 1B). Confocal imaging of confined Eps8-KD cells and analysis of re-expressed protein distribution together with FusionRed-F-tractin or -MII-RLC showed that unlike the gradient of Emerald-mEps8 with the highest level at the leader bleb base, Emerald-mEps8 Δ cap was equally distributed along the length of the leader bleb or slightly concentrated at the tip (Figure. 5E, G). Analysis of actomyosin organization showed that compared to expression of Emerald-mEps8, expression of Emerald-mEps8 Δ cap in Eps8-KD cells decreased the level of actin in the dense cortical band of the cell body, although the density gradient of actin along the leader bleb and the distribution of MII-RLC was unchanged (Figures 5E, F, G' & Figure. 5 Supplement 1). In contrast, the actin bundle anisotropy gradient in the leader bleb was highly enhanced, with Eps8-KD cells expressing Emerald-mEps8 Δ cap exhibiting nearly five-fold higher actin bundle anisotropy near the tips of their leader blebs compared to Eps8-KD cells expressing Emerald-mEps8 (Figure. 5G''). AFM analysis of cortex mechanics showed that compared to over-expression of Emerald-mEps8, over-expression of Emerald-mEps8 Δ cap significantly increased cortex tension and intracellular pressure (Figure. 5H-I & Supplementary File 1). Together, these results show that the capping activity of Eps8 decreases actin density and mechanical properties of the cortex in the cell body, but acts to antagonize actin bundle formation in the distal region of leader blebs, and together this limits leader bleb size. This further suggests that the capping activity of Eps8 may be regionally regulated to maintain a gradient of actin bundle organization in the leader bleb.

Erk activity spatially regulates actin organization to mediate leader bleb-based migration

Erk-dependent phosphorylation of Eps8 on S624 and T628 has been shown to inhibit actin capping by Eps8 without altering its filament binding activity (Menna et al., 2009), and our above results suggest that capping may be regionally regulated in melanoma cells migrating under non-adhesive confinement. Because A375 cells are known to have hyperactivation of the Erk pathway, we sought to test whether Erk activity or phospho-regulation on S624 and T628 of Eps8 regulates leader bleb formation, actin organization, and cortex mechanics. We first exploited the highly specific inhibitor U0126 to block Erk activity (Figure. 6A). We validated that U0126 inhibited Eps8 phosphorylation in A375 cells by expressing either Emerald-mEps8 or EGFP as a control, in cells treated with or without 10 μ M U0126 for 90 min, performing immunoprecipitation of the expressed proteins with anti-GFP antibodies from cell lysates, followed by western blot analysis with antibodies specific to Erk, activated Erk phosphorylated on T202/Y204, phospho-serine and phospho-threonine (pS/T). This analysis showed, as expected, that U0126 inhibited Erk activation independent of the expression of Eps8 constructs. Similarly, U0126 strongly reduced the pS/T level in immunoprecipitated Emerald-mEps8 compared to untreated cells. This indicates that U0126 blocks Erk-mediated Eps8 phosphorylation.

We then examined the role of Erk activity in cytoskeletal organization and Eps8 localization. We localized endogenous Eps8 and actin in cells plated on poly-L-Lysine to mediate non-specific adhesion during immunostaining. This showed that U0126 treatment caused cells to flatten out at their base where they attached to the coverslip and to form actin bundles in the cell center and lamellipodia and filopodia with Eps8 on their tips, although they still possessed small blebs containing Eps8 on their dorsal surface (Figures 6B & Figure. 6 Supplement 1). When cells co-expressing FusionRed-F-tractin and EGFP-MII-RLC were confined under non-adherent conditions and perfused with U0126, this remarkably induced rapid retraction of leader blebs and formation of actin bundles in the center of the

cell body that lacked myosin II (Figure. 6C & Video 6). Quantification showed that compared to untreated control, U0126 significantly reduced leader bleb area and density of the cortical actin band in the cell body, and completely blocked leader-bleb based migration (Figure. 6D, E, F). AFM analysis of cortical mechanics showed that U0126 reduced both cortical tension and intracellular pressure compared to control (Figure. 6G-H & Supplementary File 1). These results illustrate two important points. First, they show that Erk activity mediates spatial regulation of the actin cytoskeleton, such that it promotes actin density in the cortex and inhibits actin bundling in the cell center. Second, Erk activity is required for maintaining cortical tension and intracellular pressure to drive leader bleb formation for adhesion-independent migration under confinement.

MEK/Erk-mediated phosphorylation of S624 and T628 coordinates Eps8 capping and bundling activities to mediate leader bleb-based migration

We next sought to test specifically if phospho-regulation on the Erk sites (S624 and T628) of Eps8 were critical to leader bleb formation and cytoskeletal regulation. We generated a non-phosphorylatable mutant of Emerald-mEps8 (Figure. 4A, S624A/T628A, referred to as Emerald-mEps8-SATA) that has been shown to have constitutive capping activity *in vitro* and inhibit filopodia formation in neurons (Menna et al., 2009). We expressed Emerald-mEps8 or Emerald-mEps8-SATA in either control or Eps8-KD cells and subjected them to confinement under non-adhesive conditions. This showed that either reconstitution of Eps8-KD or over-expression with Emerald-mEps8-SATA blocked leader bleb formation, significantly reducing leader bleb size by ~50% and strongly inhibiting cell migration compared to expression of Emerald-mEps8 in either wild type or Eps8-KD cells (Figure. 7A-D, Supplementary File 1 & Video 7). Thus, S624 and T628 in Eps8 are required for leader bleb formation and migration under non-adhesive confinement. This further suggests that down-regulation of capping activity by phosphorylation at these sites promotes leader blebs, in agreement with our finding that the capping-deficient Eps8 Δ cap enhances leader blebs.

We then examined the effects of the Eps8 phospho-mutant on cytoskeletal organization. Interestingly, expression of Emerald-mEps8-SATA together with FusionRed-F-tractin showed that the Eps8 phospho-mutant was depleted from the cortex and instead formed thick bundle structures in the cell center (Figure. 7E), similar to the actin bundles seen in cells treated with U0126 (Figure. 6C), but the bundles were not labeled with F-tractin (Figure. 7E). However, fixation and staining with antibodies to vimentin or with fluorescent phalloidin showed that the Emerald-mEps8-SATA cables did not co-localize with intermediate filaments, but were dense with actin, suggesting that F-tractin and Eps8 may compete for the same binding site in actin bundles (Figure. 7 Supplement 1A, B). Analysis of fluorescent phalloidin intensity in the cortical band of the cell body showed that Emerald-mEps8-SATA did not alter actin density compared to Emerald-mEps8 (Figure. 7F). In addition, co-expression of Emerald-mEps8-SATA together with FusionRed MII-RLC in Eps8-KD cells showed that myosin II continued to localize to the peripheral cortex, but the central Eps8/actin bundles lacked myosin II (Figure. 7E). Quantification of the percentage of cells with Eps8/actin bundles showed that expression of F-tractin did not induce bundle formation, while over-expression of Emerald-mEps8 or Emerald-mEps8-SATA induced bundles in ~30% or ~70% of cells, respectively (Figure. 7H). This indicates that Emerald-mEps8-SATA promotes the formation of excessive non-contractile actin bundles in the cell center. Together with our previous results, this suggests that the S624 and T628 Erk phosphorylation sites in Eps8, are required for suppressing central actin bundles, while other targets of MEK/Erk regulate cortical actin density.

We then sought to determine how the S624A/T628A mutations in Eps8 mediated their effects on the cytoskeleton. We first tested whether this was due to a lack of Erk-mediated regulation on these sites. Treatment of non-adherent cells expressing either Emerald-mEps8 or Emerald-mEps8-SATA with 10 μ M U0126 for 90 min followed by fixation and phalloidin staining showed that Erk inhibition induced Eps8/actin cables to the same extent, independent of the S624A/T628A mutations (Figure. 7G, H). Because phosphorylation of S624 and T628 are known to inhibit the actin capping activity of Eps8, and yet non-phosphorylatable mutation of these sites (which would be expected to have constitutive capping) produced an ectopic actin cable effect, we wondered if the formation of Eps8/actin cables induced by Erk inhibition required either the capping or bundling activities of Eps8. Over-expression of either Emerald-mEps8 Δ cap or Emerald-mEps8 Δ bund cells in either the presence or absence of U0126 did not induce Eps8/actin cables, indicating that both capping and bundling activities are required for cable formation induced by Erk inhibition (Figure. 7G, H). Furthermore, over-expression of Emerald-mEps8 Δ cap in cells treated with U0126 and confined under agar could not rescue the loss of leader blebs induced by perfusion of Erk inhibitor (Figure. 7 Supplement 2), indicating that Erk promotes leader blebs by other mechanisms in addition to down-regulation of Eps8 capping activity. Finally, we found that over-expression of an S624E/T628E Eps8 mutant (Menna et al., 2009) could not recapitulate the effects of Emerald-mEps8 Δ cap in cells, suggesting that the E substitutions do not act as phospho-mimics to inhibit Eps8 capping activity in cells (not shown). However, together our results show that MEK/Erk-mediated phosphorylation of Eps8 on S624 and T628 inhibits the bundling- and capping-dependent formation of central actin cables by Eps8. This also suggests that in addition to directly regulating actin capping (Menna et al., 2009), these sites may affect the bundling activity of Eps8 in cells by an indirect mechanism.

We then tested the role of S624 and T628 of Eps8 and their regulation by Erk in cortex mechanics. AFM analysis showed that compared to untreated or cells expressing Emerald-mEps8, Emerald-mEps8-SATA expression reduced cortex tension and intracellular pressure to a level similar to treatment with U0126 (Figures 7I-J, 6G-H & Supplementary File 1). This was surprising, considering that this mutant had no effect on cortical actin density. However, it is possible that the cortical mechanics could be altered by the redistribution of mutant Eps8 from the cortex to central actin bundles. Together, these results suggest that Erk-mediated phosphorylation of S624 and T628 coordinates the local co-regulation of Eps8 capping and bundling activities to control cortical tension and intracellular pressure to mediate leader bleb formation and migration of confined cells.

Erk activity is concentrated in a gradient across leader blebs and its mobility is restricted by a diffusion barrier at the bleb neck

Our demonstrations that Erk activity and regional regulation of Eps8 activity are essential to leader bleb formation suggests that Erk activity itself may be regionally regulated in migrating melanoma cells. Because immunofluorescence (of phospho-Eps8 or active Erk) is not possible in cells confined under agar, we turned to a Fluorescence Resonance Energy Transfer (FRET)-based biosensor of active Erk called “Erk Kinase Activity Reporter containing EV linker” (EKAREV) (Harvey et al., 2008; Komatsu et al., 2011). In short, a CFP-tagged phospho-peptide-binding domain is connected by a FRET-optimized “EV linker” to a YFP-tagged Erk substrate peptide, and FRET is obtained when the substrate is phosphorylated by Erk. We first used the reporter to localize Erk activity in cells adhered to fibronectin-coated glass. Confocal imaging showed that EKAREV (CFP channel) was soluble, excluded

431 from membranous organelles, and diffusely localized throughout the cell, while YFP/CFP ratio imaging
432 revealed a low FRET signal indicating low Erk activity throughout the cell (Figure. 8A). In contrast, in
433 non-adherent, blebbing cells, although the EKAREV reporter was evenly distributed, the ratio image
434 showed heightened levels of FRET indicating higher Erk activity specifically in blebs (Figure. 8B, C).
435 Importantly, treatment with U0126 reduced the EKAREV FRET ratio to minimal levels (Figure. 8
436 Supplement 1). Remarkably, time-lapse ratio imaging at 5 sec intervals showed that a flash of high
437 FRET appeared in the bleb periphery just after protrusion, and was maintained until bleb retraction
438 (Figure. 8C). Thus, EKAREV reveals spatially and temporally localized Erk activity in blebs of non-
439 adherent cells.

440 We next sought to localize Erk kinase activity in non-adherent cells confined under agarose.
441 Strikingly, confocal YFP/CFP ratio imaging revealed a strong concentration of high FRET signal
442 indicating high Erk activity within leader blebs compared to the cell body (Figure. 8D & Video 8).
443 Quantification of the magnitude of FRET signal in leader bleb relative to the cell body showed >250%
444 enrichment of Erk activity in the leader bleb (Figure. 8G). Furthermore, regional analysis of the
445 magnitude of FRET signal distribution within leader blebs showed a shallow gradient, with Erk activity
446 highest at the distal tip (Figure. 8E). To determine if this effect could be caused by an enrichment of
447 signaling proteins within leader blebs, we localized either soluble EGFP, or EGFP tagged versions of
448 Erk, MEK or activated B-Raf (V600E) in cells confined under agarose (Figure. 8F). Quantification
449 showed that EGFP alone as well as EKAREV were enriched by ~10-12% in the leader bleb relative to
450 the cell body (Figure. 8G). Although Erk, MEK and B-Raf (V600E) were all enriched within leader blebs
451 by 15-20% relative to the cell body (Figure. 8F, G), this was not significantly higher than the enrichment
452 of EGFP alone. Therefore, slight enrichment of soluble proteins within leader blebs may be a general
453 phenomenon, likely because membranous organelles that exclude cytoplasmic markers are largely
454 excluded from the leader bleb and maintained in the cell body. Together, our results show that in
455 confined non-adherent cells, Erk activity is highly concentrated in leader blebs where it forms a gradient
456 with peak activity at the bleb tip.

457 Our observation that membranous organelles were excluded and soluble proteins were slightly
458 concentrated in leader blebs led us to hypothesize that leader blebs trap their contents with a diffusion
459 barrier formed by the constriction between the bleb and cell body. To test this, we utilized soluble
460 monomeric Eos which converts from green to red fluorescence upon exposure to UV light. Using a
461 localized pulse of 405 nm light, we photo-converted mEos in a rectangular region within the leader bleb
462 a short distance away from the neck and then imaged the redistribution of red fluorescence by diffusion
463 within the bleb and cell body. This showed that the majority of the red fluorescence was retained within
464 and diffused throughout the leader bleb before equilibrating with the cell body (Figure. 8H & Video 9).
465 These results indicate that the bleb neck slows diffusion of soluble components between the leader bleb
466 and cell body. Together, these results show that Erk activity concentrates in and forms a gradient
467 across leader blebs, and may be trapped there by a diffusion barrier at the bleb neck.

468 **Discussion**

469 Our study shows for the first time a critical role for Eps8 and its regulation of the actin
470 cytoskeleton in promoting cell cortex tension and intracellular pressure to induce the rapid, adhesion-
471 independent migration of confined cancer cells. We demonstrate that, in contrast to cells adhered to
472 ECM where Eps8 associates with filopodia and lamellipodia, in non-adherent melanoma cells, Eps8
473 localizes to bleb membranes as actin assemblies. A novel, bleb-based mode of migration was recently
474 described by several labs that occurs when non-adherent, highly contractile cells are squeezed in 3D
475 confinement. The pressure induced by such an environment induces cells to undergo a mesenchymal-
476 to-amoeboid transition (MAT) and adopt a characteristic polarized morphology where rapid cell motility is
477 driven by cortical cytoskeletal flow that generates extracellular friction along a large sausage-shaped
478 “leader bleb” that drags along the cell body (Bergert et al., 2015; Liu et al., 2015; Ruprecht et al., 2015).
479 We show here that in cancer cells, the actin capping and bundling scaffold protein Eps8 is required to
480 promote this morphological transition under confinement by enhancing cortical tension and promoting
481 increased intracellular pressure. Our manipulations of Eps8 level and activities that defined its
482 requirement for leader bleb formation and migration did not perturb the organization or activity of myosin
483 II. This, together with previous work (Bergert et al., 2015; Liu et al., 2015; Ruprecht et al., 2015),
484 indicates that both contractility and proper organization of the cytoskeleton are critical to generating the
485 cortical mechanical properties conducive to leader bleb-based migration under non-adhesive
486 confinement.

487 Our experimental results suggest a speculative model for how Eps8 mediates leader bleb-based
488 migration (Figure. 8I). We find that the bundling activity of Eps8 is required for promoting the
489 mesenchymal-to-leader bleb transition in confined, non-adherent melanoma cells. This identifies a
490 critical role for actin bundles in promoting the cortical inhomogeneity and cellular pressure that have
491 been postulated to mediate symmetry breaking to drive this drastic polarized cell shape change
492 (Ruprecht et al., 2015). Once the morphology transition occurs, we find that Eps8 and actin both form a
493 gradient within the leader bleb, decreasing with distance from the neck, but absent from the very tip.
494 Our demonstration the Eps8 localizes to bleb membranes on a similar timescale as ezrin suggests that
495 their interaction (Zwaenepoel et al., 2012) may be critical to Eps8 cortical recruitment. Analysis of actin
496 bundle anisotropy shows that actin bundling forms an opposing gradient, with the most organized actin
497 bundles towards the bleb tip. Actin bundles wrapping around the short axis of the bleb are likely
498 responsible for maintaining the sausage/allantoid shape. Our demonstration that inhibition of Eps8
499 capping activity further enhances actin bundle organization towards the leading bleb tip suggests that
500 Eps8’s bundling and capping activities act antagonistically, such that when capping is down-regulated,
501 Eps8 may be a more efficient bundler. Thus, local regulation of Eps8 capping activity could promote
502 polarization of actin organization with opposing gradients in actin density and bundling along the leader
503 bleb. However, by manipulating Erk activity or the Erk phosphorylation sites in Eps8, we demonstrate
504 that Erk-mediated phosphorylation of S624 and T628 not only down-regulates the capping activity of
505 Eps8 as shown previously (Menna et al., 2009), but may in fact coordinate the regulation of Eps8
506 capping and bundling activities. Our use of a FRET biosensor surprisingly shows that Erk activity is
507 massively concentrated in leader blebs, although the mechanism for this concentration is not clear.
508 However, the high activity is likely trapped there by a diffusion barrier at the bleb neck, and within the
509 leader bleb forms a shallow gradient with peak activity at the bleb tip. This suggests that Erk-mediated
510 down-regulation of Eps8 capping activity at the leader bleb tip could drive the formation of opposing

511 gradients in actin bundling and density along the bleb length. This gradient in actin organization, in turn,
512 may be required for spatial organization of cortical tension, which we predict would mirror the gradient in
513 actin bundling, to maintain the allantoid shape and drive cortical flow in the leader bleb. The increased
514 cortical tension at the bleb tip would be opposed at the bleb neck by myosin II contractility, and the
515 depletion of myosin II and actin from the very tip of the leader bleb would provide a site where high
516 intracellular pressure could promote local protrusion of the leading membrane to mediate the leader-
517 bleb-based migration of confined cells. Thus, our results identify a mechanism by which spatial
518 regulation of Eps8 actin regulatory activities by Erk may promote the rapid, unregulated migration of
519 melanoma cells that may be critical to their highly invasive behavior *in vivo*.

520 The confinement of cells simulated here by an under agarose assay is thought to occur in animal
521 cells during intraepithelial migration, within the perivascular space and between muscle fibers (Charras
522 and Sahai, 2014). Additionally, leader bleb-based migration may be important to migration between
523 tightly packed cells found in solid tumors. Our observation that inhibition of Erk activity is capable of
524 blocking formation of large leader blebs is consistent with the notion that effectors of the pathway, such
525 as Eps8, are important to the migration of confined cancer cells. The Ras/Raf/MEK/Erk pathway is one
526 of the most frequently upregulated pathways in cancer. In melanoma, this pathway is particularly active
527 because of a commonly found activating mutation in B-Raf V600E (Davies et al., 2002) that bypasses
528 Ras and the negative feedback that normally restrains MEK/Erk activity (Logue and Morrison, 2012).
529 This feature predisposes melanoma cells to blebbing by supporting a Raf/MEK/Erk/MLCK/RLC/myosin
530 contractility cascade. Drugs that target B-Raf V600E (e.g., vemurafenib) have been shown to have
531 remarkable effects in the short-term. Compensatory upregulation of the pathway by cancer cells
532 frequently limits their effectiveness (Logue and Morrison, 2012). However, our work shows that other
533 mechanisms for activating Erk, including via oncogenic Ras mutations in lung cancer cells or via serum
534 factors in osteosarcoma cells also lead to Eps8-dependent bleb-based migration. The work described
535 here elucidates the importance of a specific Erk effector, Eps8, in the migration of confined melanoma
536 cells. Therefore, targeting specific effectors as opposed to canonical signaling enzymes may have
537 therapeutic value. Effectors that impact cell architecture through the regulation of the cytoskeleton could
538 be particularly attractive targets especially for prevention of metastasis.

539 **METHODS**

540 **Cell culture and transfection**

541 A375, A549 and U2OS cells were all obtained from American Type Culture Collection (ATCC)
542 and all were maintained for up to 15 passages in DMEM supplemented with 10% FBS, GlutaMAX (Life
543 Technologies), antibiotic-antimycotic (Life Technologies) and 20 mM Hepes pH 7.4. Lipofectamine 2000
544 (Life Technologies) and RNAiMAX (Life Technologies) were used to transfect plasmids and small
545 interfering RNAs, respectively. Cells were plated on 6-well glass bottom plates (In Vitro Scientific) either
546 directly, or after coating with either 5 or 50 µg/ml human plasma fibronectin (Millipore) or poly-L-Lysine
547 (Millipore), as noted.

548 **Confinement of cells under agarose**

549 Agarose slabs for cell confinement (Bergert et al., 2012) were made by adding 750 mg of
550 ultrapure agarose (Life Technologies) to 50 mL of 20 mM Hepes (pH 7.4), microwaving briefly, and
551 pouring 4 mL into each well of a 6-well glass bottom plate (In Vitro Scientific). After gelation, a hole was
552 punched in the agarose using a 5 mL plastic test tube. Prior to confining cells, 3 mL of media was
553 pipetted into each well and equilibrated with the agarose overnight. Before use, media was thoroughly
554 vacuumed off and 200 microliters of media containing cells was added to the empty hole punch. To get
555 cells under the agarose, a 1 mL pipette tip was placed into the hole punch containing media and cells
556 and slid just under the agarose to gently lift a portion of the agarose, sucking the cells underneath, and
557 the pad was gently set down. The remaining media and cells were then thoroughly vacuumed out of the
558 hole punch. To prevent drying, the plate was sealed using parafilm. Prior to imaging, the plate was
559 brought up to temperature for 1 hr in an incubator.

560 **Pharmacological treatments**

561 To inhibit the Erk pathway, a working concentration of 10 µM U0126 (Cell Signaling Technology)
562 was prepared by diluting a 1000X stock solution in DMSO into complete media and dissolved using a
563 vortex mixer for 30 sec before adding to cells. Phospho-Erk (T202/Y204) (#4370) and Erk (#9102)
564 antibodies purchased from Cell Signaling Technology were used to confirm inhibition of MEK by
565 Western blotting of whole-cell lysates. Cells were treated with U0126 for 30 min for AFM assays and 90
566 min for light microscopy assays. Cells under agarose were treated by applying media containing U0126
567 directly on top of the agar pad. Blebbistatin (Sigma Aldrich) was used at 50 µM and applied directly to
568 the cells for 5 min before AFM analyses.

569 **Plasmids**

570 EGFP-tagged mouse Eps8 (GFP-mEps8) and Emerald-mEps8-SATA (S624A/T628A) were the kind gift
571 of Giorgio Scita (University of Milan). Bundling (L757A/K759A, *Δbund*) and capping (V689D/L693D,
572 *Δcap*) defective versions of Emerald-mEps8 were made using Quick Change II XL (Agilent
573 Technologies) and the following primers:

574 *Δbund*

575 Forward primer: CGGAGCACAACTCTTTTCTGCCAACGCAGACGAACTGAGGTCTG

576 Reverse primer: CAGACCTCAGTTCGTCTGCGTTGGCAGAAAAGAGTTGTGCTCCG

577 *Δcap*

578 Forward primer: GTCCCAGATGGAAGAGGATCAGGATGAGGACTTCCAGAGGCTGACC

579 Reverse primer: GGTCAGCCTCTGGAAGTCCTCATCCTGATCCTCTTCCATCTGGGAC

580 Open reading frames of WT, non-phosphorylatable, *Δbund* and *Δcap* versions of mEps8 were then PCR
581 amplified and inserted into pENTR/D-TOPO (Life Technologies) before shuttling into pcDNA 6.2/N-
582 EmGFP-DEST (Life Technologies) using LR Clonase (Life Technologies).

583 mEmerald and Fusion Red-tagged F-tractin, an acting binding peptide derived from the Itpka
584 protein from rat [] was generated by cloning into a Clontech-style vector containing the advanced EGFP
585 variant Emerald (F64L, S65T, S72A, N149K, M153T, I167T, A206K). The following primers were used
586 to amplify F-tractin from rat Itpka (NM_031045.2) and generate a 13 amino acid linker separating the F-
587 tractin from the fluorescent protein:

588 Forward primer containing HindIII site: AGC TCA AGC TTA TGG GCA TGG CGC GAC CAC GGG GCG
589 C

590 Reverse primer containing BamHI site: CCG GTG GAT CCG ATC CAG ATC CGC CGC AGC GCG CTT
591 CGA AGA GCA GGC GCA GCT CC

592 The resulting PCR product and mEmerald-N1 were digested by the appropriate restriction enzymes, gel
593 purified, and ligated to yield mEmerald-F-tractin-N-13. Upon sequence verification of the vector,
594 mEmerald-F-tractin-N-13, and FusionRed-N1 were digested by the appropriate restriction enzymes, gel
595 purified, and ligated to yield FusionRed-F-tractin-N-13.

596 EKAREV was kindly provided by Kazuhiro Aoki (Kyoto University) and Jun-ichi Miyazaki (Osaka
597 University), EGFP-B-Raf V600E was generated by the Advanced Technology Research Facility (NCI,
598 Frederick, MD). Ezrin-GFP (Stephen Shaw), EGFP-Erk1 (Rony Seger), MEK1-GFP (Rony Seger) and
599 mEos2 (Michael Davidson) were obtained from Addgene. FusionRed tagged myosin II regulatory light
600 chain (RLC) and vimentin were purchased from Evrogen.

601 **siRNA knockdown of endogenous human Eps8**

602 The human-specific Eps8 siRNA (#4392420) used during this study was from Life Technologies.
603 Cells were incubated with siRNA for 24 hr prior to performing experiments. Knockdown was confirmed
604 by Western blotting of whole-cell lysates for the presence of Eps8.

605 **Western blotting**

606 Whole-cell lysates were prepared by scraping cells into ice cold RIPA buffer (50 mM Hepes pH 7.4, 150
607 mM NaCl, 5 mM EDTA, 0.1% SDS, 0.5% deoxycholate and 1% Triton X-100) containing protease and
608 phosphatase inhibitors (Roche). Before loading onto 4-12% NuPAGE Bis-Tris gradient gels (Life
609 Technologies), lysates were cleared by centrifugation. Following SDS-PAGE, proteins in gels were
610 transferred to nitrocellulose using an iBlot (Life Technologies). Before blocking, proteins were fixed to

the nitrocellulose by air drying the membrane overnight at room temperature. Blocking of membranes was then done in blocking buffer (Hepes buffered saline containing 0.1% Triton X-100, 1% BSA, 1% fish gelatin and 5 mM EDTA). Antibodies against Eps8 (BD Biosciences #610143), phospho-Erk (Cell Signaling Technology #4370), Erk (Cell Signaling Technology #9102), pMLC (Rockland #600-401-416) and MLC (Rockland #600-401-938) were used at a 1:1000 dilution and incubated overnight at 4°C in blocking buffer. IRDye 680RD and 800CW secondary antibodies (LI-COR Biosciences) were then used at 1:5000 in blocking buffer for 2 hr at room temperature after extensive washing in Hepes Buffered Saline (HBS) containing 0.1% Triton X-100. Bands were then resolved on an Odyssey scanner (LI-COR Biosciences).

Immunoprecipitations

12 hr after transfection of plasmids encoding EGFP or Emerald-tagged mouse Eps8, A375 whole-cell lysates were prepared by scraping into ice cold RIPA buffer (50 mM Hepes pH 7.4, 150 mM NaCl, 5 mM EDTA, 0.1% SDS, 0.5% deoxycholate and 1% Triton X-100) containing protease and phosphatase inhibitors (Roche). Before immunoprecipitation, lysates were cleared by centrifugation. EGFP and Emerald tagged proteins were immunoprecipitated using a mouse GFP antibody (Roche Life Sciences #11814460001) and Protein-G magnetic beads (Life Technologies) for 2 hr at 4 °C. Immunoprecipitated proteins were washed four times with ice cold RIPA buffer before running on 4-12% NuPAGE Bis-Tris gradient gels (Life Technologies). Following SDS-PAGE, proteins in gels were electrotransferred to nitrocellulose using an iBlot (Life Technologies). For U0126 treatments, A375 cells were treated with 10 µM U0126 for 90 min and inhibition of Erk activity was confirmed by Western blotting for phospho-Erk and Erk as described under “Western blotting.” Proteins with phosphorylated serine or threonine were detected using a rabbit anti-pS/T antibody (Abcam #ab17464) used at 1:500. Immunoprecipitated EGFP and Emerald tagged proteins was confirmed using a rabbit GFP antibody (Life Technologies #A6455) used at 1:1000.

Immunofluorescence

Cells were cultured, stained and imaged in 6-well glass bottom dishes (In Vitro Scientific). Where noted, glass was first coated with 5 or 50 µg/mL human plasma fibronectin (Millipore) or poly-L-Lysine (Millipore) for 1 hr at 37°C. Samples were fixed using 4% paraformaldehyde (Electron Microscopy Sciences) in HBS for 20 min at room temperature. Permeabilization/blocking were performed using blocking buffer for an hour. Eps8 antibody (BD Biosciences #610143) was used at a 1:250 dilution, fluorescently conjugated phalloidin (Life Technologies) at 1:200, and fluorescently conjugated wheat germ agglutinin (Life Technologies) at 1:1000. Each was incubated in blocking buffer overnight at room temperature. Samples were gently washed several times in HBS containing 0.1% Triton X-100. An anti-mouse Alexa Fluor 488 secondary antibody (Life Technologies) was used to detect Eps8. Imaging was performed in HBS.

Light Microscopy

Immunofluorescence and time-lapse live-cell fluorescence microscopy was performed using the imaging system that is described in (Shin, 2010). Briefly, this consisted of an automated Eclipse Ti microscope equipped with the Perfect Focus System (Nikon), a servomotor driven X-Y stage with a piezo top plate (Applied Scientific Instruments) and a CSU-X1-A3 spinning disk confocal scan head

(Yokogawa). Illumination for confocal imaging was provided by solid state lasers (40 mW 442 nm for CFP; 100 mW 488 nm for EGFP; 100 mW 523 nm for YFP and 500 mW 561 nm for FusionRed) that were directed to the microscope by a custom-designed optical fiber-coupled laser combiner (Shin, 2010). For phase contrast imaging, illumination was provided by a quartz-halogen lamp using a 546 nm bandpass filter. Images were acquired using either a CoolSNAP HQ2 or MYO cooled CCD camera (Photometrics) using either a 100X or 60X (1.4 NA, Plan Apo PH) oil immersion objective lens and 0.9 NA phase-contrast optics. Illumination, image acquisition, and microscope functions were controlled by Metamorph software (Molecular Devices). For time-lapse FRET imaging of the EKAREV biosensor, a confocal image through the central plane of the cell was first acquired using 442 nm excitation and the YFP emission filter (FRET image), followed by an image acquired using 442 nm excitation and the CFP emission filter (CFP image). For photo-activation of mEos2, a Nikon A1R laser-scanning confocal microscope equipped with dual resonant scanners was used with a 60X (1.4 NA Plan Fluor) oil immersion lens. A 0.5 second pulse of the 405 nm laser at 50% power within a defined region was used to photo-convert mEos2. Images were then acquired using the 488 and 561 nm lasers in the red and green channels at 130 ms intervals to image the redistribution of fluorescence after photo-conversion. For all experiments, a stage-top incubator (Tokai-Hit) was used to maintain samples at 37C.

Measurement of the timing of protein accumulation on bleb membranes

Cells expressing EGFP or Emerald-tagged protein were plated on uncoated 6-well glass bottom plates (In Vitro Scientific) in media containing 0.1 mg/mL rhodamine-labeled dextran (MW = 70 kDa, Sigma Aldrich). Time of arrival along the bleb perimeter was determined to be when EGFP or Emerald fluorescence was above background. Maximal protrusion of the bleb membrane as judged by displacement of rhodamine-dextran (negative stain) was set as time 0.

Measurement of leader bleb area and percent cell migration

For determination of leader bleb area, confocal images of EGFP or Emerald through the central plane of confined cells were acquired for 4 hr at 5 min intervals. Leader bleb and cell body area were measured using images of soluble EGFP for non-targeting and hEps8 siRNA treated cells and Emerald tagged to Eps8 in rescue and over-expression experiments by outlining cells in each frame using Fiji (<http://fiji.sc/Fiji>). The percent of migratory cells was determined from time-lapse phase contrast images acquired for 4 hr at 5 min intervals. The number of moving versus stationary cells was counted during the course of the Video.

Measurement of actin cortex density and thickness

Round cells on uncoated 6-well glass bottom plates were prepared as described in “immunofluorescence.” To measure actin cortex density, cells were stained with Alexa Fluor 568 conjugated phalloidin (Life Technologies). To measure cortex thickness, we used the methods of (Clark et al., 2013). Briefly, cells were double-labeled with Alexa Fluor 568-conjugated wheat germ agglutinin (Life Technologies) and Alexa Fluor 647-conjugated phalloidin. Spinning disk confocal images through the central Z-plane of the cell were acquired using a 100X (1.4 NA) objective lens. For cortex density, a 5 pixel wide line was drawn along a region of the cortex that was free of blebs and the mean fluorescence intensity was measured using Fiji (<http://fiji.sc/Fiji>). Additionally, background fluorescence was measured by selecting a region inside the cell. Actin cortex density was then calculated as the

691
692
693
694
695

696

697
698
699
700
701

702

703
704
705
706
707
708
709

710

711
712
713
714
715
716
717
718
719
720
721
722
723
724
725

726

727
728
729

mean fluorescence intensity at the cortex minus background fluorescence. For determining cortex thickness, images were analyzed by performing an intensity line-scan perpendicular to and across the cell edge on a dual color image, and the distance between the peaks of the phalloidin and wheat germ agglutinin fluorescence intensity was recorded and input into the equation reported by Clark *et al.* 2013 to calculate the cortex thickness.

Measurement of the distribution and anisotropy of proteins in leader blebs

For regional analyses of protein distribution and anisotropy, five regions of Interest (ROIs) each representing 20% of the length of the leader bleb were drawn using Fiji (<http://fiji.sc/Fiji>). Using FibrilTool (Boudaoud et al., 2014), we measured the anisotropy of F-actin fluorescence signal within the same regions used for determining protein distribution. FusionRed-F-actin images having similar contrast, as determined by SD/mean, were used for anisotropy analyses.

FRET and mEos2 photo-conversion image analysis

To generate emission ratio images, we wrote a Fiji (<http://fiji.sc/Fiji>) macro based on previously described work (Pertz et al., 2006). Briefly, CFP and FRET images were first background-subtracted and corrected for bleaching by exponential fitting. CFP images were then thresholded to generate a binary mask. After multiplication by this mask, the FRET image was divided by the CFP image to yield an emission ratio reflecting Erk kinase activity throughout the cell. Ratio images were then pseudo colored using the “16 color” LUT. Similarly, images of diffusing mEos2 were pseudo colored using the “16 color” LUT.

Atomic force microscopy

Force spectroscopy on non-adherent cells was performed using a Bioscope II AFM system (Veeco) mounted on an automated inverted epi-fluorescence microscope (Nikon Eclipse TE2000) controlled by Metamorph software (Molecular Devices). Illumination was provided by a mercury arc lamp and wavelengths selected by a Sedat filterset (Semrock). The hybrid microscope instrument was placed on an acoustic isolation table (Kinetic Systems). A heating stage (Veeco) was used to maintain cells at 37C. Cells were located by EGFP fluorescence while cell radii were measured using bright-field images taken with a 40X (0.6 NA Plan Fluor) objective lens and a QuantEM EMCCD camera (Photometrics). After location of cells, a soft and tipless rectangular silicon nitride cantilever (length: 350 +/- 5 µm, width: 32.5 +/- 3 µm, thickness: 1 +/- 0.5 µm; MikroMasch) was brought to close proximity. The cantilever stiffness was first calibrated by performing a force curve on the stiffer glass-bottom dish to estimate the photodetector deflection sensitivity, and then by using the thermal noise fluctuation method (Hutter and Bechhoefer, 1993). The estimated spring constants for cantilevers used in force curves were 0.08-0.11 N/m. After calibration, the AFM cantilever was moved on top of a cell and lowered to gently deform it. Approximately ten successive force curves were performed in the same location on each cell per condition using 4 µm ramps with up to ~1 nN applied force at 0.5 Hz.

Analysis of atomic force microscopy data

All AFM force spectroscopy measurements were analyzed to extract the cell mechanical properties using MATLAB (Mathworks). Before importing the force curves into MATLAB for analysis, each individual acquired curve was preconditioned by offsetting the y-axis to 0 and reformatted to a text

730 file format using the NanoScope Analysis software (Bruker). We discarded noisy force curves and/or
731 curves that presented jumps possibly due to cantilever slippage or very weakly adhered and moving
732 rounded cells. For initial contact estimation, user-dependent determination was employed, selecting the
733 location when the force curves increased substantially from zero. This method does not required prior
734 knowledge or assumption about the material and geometrical properties of the cell. For fitting, Z
735 distances between 0-400 nm were relatively consistent in yielding good fits ($R^2>0.9$). Curves with poor
736 fits $R^2<0.9$ were discarded from the analysis.

737 **Determination of cortical tension and intracellular pressure**

738 A simple theory was derived for the quantitative determination of mechanical properties of non-
739 adherent melanoma cells confined between two flat surfaces. This is described in detail elsewhere
740 (manuscript under review). Briefly, when a spherical cell is rapidly (0.5 Hz) but gently pressed down
741 upon by the soft tipless cantilever, the cell is assumed to deform to an ellipsoid shape. The surface
742 tension can be estimated by force balance in the vertical Z-direction. This force balance enables the
743 relationship of the external applied cantilever force to the internal hydrostatic pressure and cortical
744 tension. The Laplace's law describes the proportional relationship between tension and pressure. The
745 derived expressions for the cortical tension and intracellular pressure of a non-adherent cell are

$$746 \quad T = \frac{k_c}{\pi} \left(\frac{1}{Z/d^{-1}} \right), \quad (S1)$$

$$747 \quad P = \frac{2T}{R}, \quad (S2)$$

748 where T is the cortical tension, P is the intracellular pressure, k_c is the calibrated effective cantilever
749 spring constant, Z is the Z-piezo extension distance, d is the cantilever deflection and R is the sample
750 radius.

751 **Statistics**

752 Statistical significance between means was determined using a two-tailed Student's t-test in
753 GraphPad Prism. All differences were considered significant if $p \leq 0.05$.

754 **Acknowledgements**

755 We thank Bill Shin for maintenance of the Waterman lab microscopes and Schwanna Thacker
756 for administrative assistance. We thank Ewa Paluch (UCL) for valuable discussions, Giorgio Scita
757 (University of Milan) for providing WT and non-phosphorylatable Eps8, and Kazuhiro Aoki (Kyoto
758 University) and Jun-ichi Miyazaki (Osaka University) for EKAREV plasmid DNA. We are grateful to the
759 Advanced Technology Research Facility (Frederick, MD) for generating EGFP-B-Raf V600E and the
760 NHLBI light microscopy core facility for use of the Nikon A-1R. This work was supported by funds from
761 the intramural research program at the NIH.

762 **Author contributions**

763 JSL, CMW, and RSC conceived the study. JSL performed all experiments and analyzed results except
764 for AFM. AXC performed AFM experiments and analyzed results. MAB and MWD designed and
765 generated fluorescent protein tagged F-tractin expression vectors. RSC derived the equation for the
766 mechanical properties of round cells. CMW and JSL wrote the paper with comments from RSC and
767 AXC.

768 **Competing financial interests**

769 The authors declare no competing financial interests.

770 **References**

771 Bergert, M., S.D. Chandradoss, R.A. Desai, and E. Paluch. 2012. Cell mechanics control rapid
772 transitions between blebs and lamellipodia during migration. *Proc Natl Acad Sci U S A*.
773 109:14434-14439.

774 Bergert, M., A. Erzberger, R.A. Desai, I.M. Aspalter, A.C. Oates, G. Charras, G. Salbreux, and E.K.
775 Paluch. 2015. Force transmission during adhesion-independent migration. *Nat Cell Biol*. 17:524-
776 529.

777 Boudaoud, A., A. Burian, D. Borowska-Wykret, M. Uyttewaal, R. Wrzalik, D. Kwiatkowska, and O.
778 Hamant. 2014. FibrilTool, an ImageJ plug-in to quantify fibrillar structures in raw microscopy
779 images. *Nat Protoc*. 9:457-463.

780 Charras, G., and E. Paluch. 2008. Blebs lead the way: how to migrate without lamellipodia. *Nat Rev Mol*
781 *Cell Biol*. 9:730-736.

782 Charras, G., and E. Sahai. 2014. Physical influences of the extracellular environment on cell migration.
783 *Nat Rev Mol Cell Biol*. 15:813-824.

784 Charras, G.T., C.K. Hu, M. Coughlin, and T.J. Mitchison. 2006. Reassembly of contractile actin cortex in
785 cell blebs. *J Cell Biol*. 175:477-490.

786 Charras, G.T., J.C. Yarrow, M.A. Horton, L. Mahadevan, and T.J. Mitchison. 2005. Non-equilibration of
787 hydrostatic pressure in blebbing cells. *Nature*. 435:365-369.

788 Clark, A.G., K. Dierkes, and E.K. Paluch. 2013. Monitoring actin cortex thickness in live cells. *Biophys J*.
789 105:570-580.

790 Davies, H., G.R. Bignell, C. Cox, P. Stephens, S. Edkins, S. Clegg, J. Teague, H. Woffendin, M.J.
791 Garnett, W. Bottomley, N. Davis, E. Dicks, R. Ewing, Y. Floyd, K. Gray, S. Hall, R. Hawes, J.
792 Hughes, V. Kosmidou, A. Menzies, C. Mould, A. Parker, C. Stevens, S. Watt, S. Hooper, R.
793 Wilson, H. Jayatilake, B.A. Gusterson, C. Cooper, J. Shipley, D. Hargrave, K. Pritchard-Jones, N.
794 Maitland, G. Chenevix-Trench, G.J. Riggins, D.D. Bigner, G. Palmieri, A. Cossu, A. Flanagan, A.
795 Nicholson, J.W. Ho, S.Y. Leung, S.T. Yuen, B.L. Weber, H.F. Seigler, T.L. Darrow, H. Paterson,
796 R. Marais, C.J. Marshall, R. Wooster, M.R. Stratton, and P.A. Futreal. 2002. Mutations of the
797 BRAF gene in human cancer. *Nature*. 417:949-954.

798 Disanza, A., M.F. Carlier, T.E. Stradal, D. Didry, E. Frittoli, S. Confalonieri, A. Croce, J. Wehland, P.P. Di
799 Fiore, and G. Scita. 2004. Eps8 controls actin-based motility by capping the barbed ends of actin
800 filaments. *Nat Cell Biol*. 6:1180-1188.

801 Disanza, A., S. Mantoani, M. Hertzog, S. Gerboth, E. Frittoli, A. Steffen, K. Berhoerster, H.J.
802 Kreienkamp, F. Milanesi, P.P. Di Fiore, A. Ciliberto, T.E. Stradal, and G. Scita. 2006. Regulation
803 of cell shape by Cdc42 is mediated by the synergic actin-bundling activity of the Eps8-IRSp53
804 complex. *Nat Cell Biol*. 8:1337-1347.

805 Downward, J. 2003. Targeting RAS signalling pathways in cancer therapy. *Nat Rev Cancer*. 3:11-22.

806 Esteche, A., L. Sanchez-Martin, A. Puig-Kroger, R.A. Bartolome, J. Teixido, R. Samaniego, and P.
807 Sanchez-Mateos. 2009. Moesin orchestrates cortical polarity of melanoma tumour cells to initiate
808 3D invasion. *J Cell Sci*. 122:3492-3501.

809 Fazioli, F., L. Minichiello, V. Matoska, P. Castagnino, T. Miki, W.T. Wong, and P.P. Di Fiore. 1993. Eps8,
810 a substrate for the epidermal growth factor receptor kinase, enhances EGF-dependent mitogenic
811 signals. *EMBO J*. 12:3799-3808.

812 Fischer-Friedrich, E., A.A. Hyman, F. Julicher, D.J. Muller, and J. Helenius. 2014. Quantification of
813 surface tension and internal pressure generated by single mitotic cells. *Sci Rep*. 4:6213.

814 Griffith, O.L., A. Melck, S.J. Jones, and S.M. Wiseman. 2006. Meta-analysis and meta-review of thyroid
815 cancer gene expression profiling studies identifies important diagnostic biomarkers. *J Clin Oncol*.
816 24:5043-5051.

817 Harvey, C.D., A.G. Ehrhardt, C. Cellurale, H. Zhong, R. Yasuda, R.J. Davis, and K. Svoboda. 2008. A
818 genetically encoded fluorescent sensor of ERK activity. *Proc Natl Acad Sci U S A*. 105:19264-
819 19269.

- Hertzog, M., F. Milanese, L. Hazelwood, A. Disanza, H. Liu, E. Perlade, M.G. Malabarba, S. Pasqualato, A. Maiolica, S. Confalonieri, C. Le Clainche, N. Offenhauser, J. Block, K. Rottner, P.P. Di Fiore, M.F. Carlier, N. Volkmann, D. Hanein, and G. Scita. 2010. Molecular basis for the dual function of Eps8 on actin dynamics: bundling and capping. *PLoS Biol.* 8:e1000387.
- Hutter, J.L., and J. Bechhoefer. 1993. Calibration of Atomic-Force Microscope Tips (Vol 64, Pg 1868, 1993). *Review of Scientific Instruments.* 64:3342-3342.
- Jain, R.K. 1987. Transport of molecules in the tumor interstitium: a review. *Cancer Res.* 47:3039-3051.
- Kang, H., C.S. Wilson, R.C. Harvey, I.M. Chen, M.H. Murphy, S.R. Atlas, E.J. Bedrick, M. Devidas, A.J. Carroll, B.W. Robinson, R.W. Stam, M.G. Valsecchi, R. Pieters, N.A. Heerema, J.M. Hilden, C.A. Felix, G.H. Reaman, B. Camitta, N. Winick, W.L. Carroll, Z.E. Dreyer, S.P. Hunger, and C.L. Willman. 2012. Gene expression profiles predictive of outcome and age in infant acute lymphoblastic leukemia: a Children's Oncology Group study. *Blood.* 119:1872-1881.
- Kishan, K.V., G. Scita, W.T. Wong, P.P. Di Fiore, and M.E. Newcomer. 1997. The SH3 domain of Eps8 exists as a novel intertwined dimer. *Nat Struct Biol.* 4:739-743.
- Klemke, R.L., S. Cai, A.L. Giannini, P.J. Gallagher, P. de Lanerolle, and D.A. Cheresh. 1997. Regulation of cell motility by mitogen-activated protein kinase. *J Cell Biol.* 137:481-492.
- Komatsu, N., K. Aoki, M. Yamada, H. Yukinaga, Y. Fujita, Y. Kamioka, and M. Matsuda. 2011. Development of an optimized backbone of FRET biosensors for kinases and GTPases. *Mol Biol Cell.* 22:4647-4656.
- Lamallice, L., F. Le Boeuf, and J. Huot. 2007. Endothelial cell migration during angiogenesis. *Circ Res.* 100:782-794.
- Lammermann, T., B.L. Bader, S.J. Monkley, T. Worbs, R. Wedlich-Soldner, K. Hirsch, M. Keller, R. Forster, D.R. Critchley, R. Fassler, and M. Sixt. 2008. Rapid leukocyte migration by integrin-independent flowing and squeezing. *Nature.* 453:51-55.
- Lammermann, T., and M. Sixt. 2009. Mechanical modes of 'amoeboid' cell migration. *Curr Opin Cell Biol.* 21:636-644.
- Lauffenburger, D.A., and A.F. Horwitz. 1996. Cell migration: a physically integrated molecular process. *Cell.* 84:359-369.
- Lie, P.P., D.D. Mruk, W.M. Lee, and C.Y. Cheng. 2009. Epidermal growth factor receptor pathway substrate 8 (Eps8) is a novel regulator of cell adhesion and the blood-testis barrier integrity in the seminiferous epithelium. *FASEB J.* 23:2555-2567.
- Liu, Y.J., M. Le Berre, F. Lautenschlaeger, P. Maiuri, A. Callan-Jones, M. Heuze, T. Takaki, R. Voituriez, and M. Piel. 2015. Confinement and low adhesion induce fast amoeboid migration of slow mesenchymal cells. *Cell.* 160:659-672.
- Logue, J.S., and D.K. Morrison. 2012. Complexity in the signaling network: insights from the use of targeted inhibitors in cancer therapy. *Genes Dev.* 26:641-650.
- Lorentzen, A., J. Bamber, A. Sadok, I. Elson-Schwab, and C.J. Marshall. 2011. An ezrin-rich, rigid uropod-like structure directs movement of amoeboid blebbing cells. *J Cell Sci.* 124:1256-1267.
- Manor, U., A. Disanza, M. Grati, L. Andrade, H. Lin, P.P. Di Fiore, G. Scita, and B. Kachar. 2011. Regulation of stereocilia length by myosin XVa and whirlin depends on the actin-regulatory protein Eps8. *Curr Biol.* 21:167-172.
- Menna, E., A. Disanza, C. Cagnoli, U. Schenk, G. Gelsomino, E. Frittoli, M. Hertzog, N. Offenhauser, C. Sawallisch, H.J. Kreienkamp, F.B. Gertler, P.P. Di Fiore, G. Scita, and M. Matteoli. 2009. Eps8 regulates axonal filopodia in hippocampal neurons in response to brain-derived neurotrophic factor (BDNF). *PLoS Biol.* 7:e1000138.
- Menna, E., S. Zambetti, R. Morini, A. Donzelli, A. Disanza, D. Calvigioni, D. Braidà, C. Nicolini, M. Orlando, G. Fossati, M. Cristina Regondi, L. Pattini, C. Frassoni, M. Francolini, G. Scita, M. Sala, M. Fahnstock, and M. Matteoli. 2013. Eps8 controls dendritic spine density and synaptic plasticity through its actin-capping activity. *EMBO J.* 32:1730-1744.
- Papusheva, E., and C.P. Heisenberg. 2010. Spatial organization of adhesion: force-dependent regulation and function in tissue morphogenesis. *EMBO J.* 29:2753-2768.

- Pertz, O., L. Hodgson, R.L. Klemke, and K.M. Hahn. 2006. Spatiotemporal dynamics of RhoA activity in migrating cells. *Nature*. 440:1069-1072.
- Podlubnaya, Z.A., L.A. Tskhovrebova, M.M. Zaalishvili, and G.A. Stefanenko. 1975. Electron microscopic study of alpha-actinin. *J Mol Biol*. 92:357-359.
- Ramanathan, S.P., J. Helenius, M.P. Stewart, C.J. Cattin, A.A. Hyman, and D.J. Muller. 2015. Cdk1-dependent mitotic enrichment of cortical myosin II promotes cell rounding against confinement. *Nat Cell Biol*. 17:148-159.
- Roberts, P.J., and C.J. Der. 2007. Targeting the Raf-MEK-ERK mitogen-activated protein kinase cascade for the treatment of cancer. *Oncogene*. 26:3291-3310.
- Ruprecht, V., S. Wieser, A. Callan-Jones, M. Smutny, H. Morita, K. Sako, V. Barone, M. Ritsch-Marte, M. Sixt, R. Voituriez, and C.P. Heisenberg. 2015. Cortical contractility triggers a stochastic switch to fast amoeboid cell motility. *Cell*. 160:673-685.
- Schell, M.J., C. Erneux, and R.F. Irvine. 2001. Inositol 1,4,5-trisphosphate 3-kinase A associates with F-actin and dendritic spines via its N terminus. *J Biol Chem*. 276:37537-37546.
- Scita, G., J. Nordstrom, R. Carbone, P. Tenca, G. Giardina, S. Gutkind, M. Bjarnegard, C. Betsholtz, and P.P. Di Fiore. 1999. EPS8 and E3B1 transduce signals from Ras to Rac. *Nature*. 401:290-293.
- Shin, W.D., Fischer R.S., Kanchawong P., Kim Y., Lim J., Myers, K.A., Nishimura Y., Plotnikov S.V., Thievensen I., Yarar D., Sabass B., Waterman C.M. 2010. A versatile, multicolor total internal reflection fluorescence and spinning-disk confocal microscope system for high-resolution live cell imaging. *In* Live cell imaging: A laboratory manual. S.J. Goldman RD, Spector DL, editor. Cold Spring Harbor Laboratory Press, Cold Spring Harbor. 119-138.
- Tinevez, J.Y., U. Schulze, G. Salbreux, J. Roensch, J.F. Joanny, and E. Paluch. 2009. Role of cortical tension in bleb growth. *Proc Natl Acad Sci U S A*. 106:18581-18586.
- Tozluoglu, M., A.L. Tournier, R.P. Jenkins, S. Hooper, P.A. Bates, and E. Sahai. 2013. Matrix geometry determines optimal cancer cell migration strategy and modulates response to interventions. *Nat Cell Biol*. 15:751-762.
- Vicente-Manzanares, M., X. Ma, R.S. Adelstein, and A.R. Horwitz. 2009. Non-muscle myosin II takes centre stage in cell adhesion and migration. *Nat Rev Mol Cell Biol*. 10:778-790.
- Wang, H., V. Patel, H. Miyazaki, J.S. Gutkind, and W.A. Yeudall. 2009. Role for EPS8 in squamous carcinogenesis. *Carcinogenesis*. 30:165-174.
- Waterman, C.M., and C. Skau. 2015. Specification of Architecture and Function of Actin Structures by Actin Nucleation Factors. *Annual Review of Biophysics*. 44:null.
- Werner, A., A. Disanza, N. Reifenberger, G. Habeck, J. Becker, M. Calabrese, H. Urlaub, H. Lorenz, B. Schulman, G. Scita, and F. Melchior. 2013. SCFFbxw5 mediates transient degradation of actin remodeller Eps8 to allow proper mitotic progression. *Nat Cell Biol*. 15:179-188.
- Zwaenepoel, I., A. Naba, M.M. Da Cunha, L. Del Maestro, E. Formstecher, D. Louvard, and M. Arpin. 2012. Ezrin regulates microvillus morphogenesis by promoting distinct activities of Eps8 proteins. *Mol Biol Cell*. 23:1080-1094.

911 **Figure Legends**

912 **Figure 1. Eps8 is recruited early to bleb membranes and forms a gradient across the length of a**
913 **“leader bleb.”**

914 (A) Confocal image of the ventral Z-plane of human A375 melanoma cells expressing Emerald-
915 tagged mouse Eps8 (green) plated on fibronectin-coated glass and stained with phalloidin (red). (B-G)
916 Confocal images through the central Z-plane of A375 cells plated on uncoated glass. (B) Cell
917 expressing Emerald-mEps8. (C) Time-lapse series of Emerald-mEps8 (green) and rhodamine-dextran
918 (red) used as a negative stain in the culture media to detect the position of the cell membrane. Times in
919 (C,E,G) indicate seconds after the formation of a new bleb. (D) Cell expressing Emerald-tagged F-
920 tractin to label actin filaments. (E) Time-lapse series of Emerald-F-tractin and rhodamine-dextran. (F)
921 Cell expressing EGFP-tagged myosin II regulatory light chain (EGFP-RLC). (G) Time-lapse series of
922 EGFP-RLC and rhodamine-dextran. (H) Quantification of the average time of appearance of EGFP or
923 Emerald-tagged cortical proteins (EGFP-Ezrin, Emerald-mEps8, Emerald-F-tractin, and EGFP-RLC)
924 relative to the time of maximal membrane protrusion determined from time-lapse series similar to those
925 shown in (C, E, G, and S1B)). (I-K-N) Confocal images through the ventral Z-plane of A375 cells plated
926 on uncoated glass and confined under an agar slab. (I) Cell co-expressing Emerald-mEps8 (green) and
927 FusionRed-F-tractin (red). Boxed area is shown zoomed in (K). (J) Average ratio of fluorescence in the
928 leader bleb to that in the cell body for Emerald-mEps8 and FusionRed-F-tractin. (K) (Left) Example of 5
929 regions of interest (ROIs), each 20% of the length of the leader bleb, used for (Right) regional analysis
930 of the average fluorescence (normalized to maximum) of Emerald-mEps8 (green) and FusionRed-F-
931 tractin (red) along leader blebs. (L) (Left) Image and (right) regional analysis of FusionRed-RLC (red)
932 and Emerald-mEps8 (green, image not shown) fluorescence in leader blebs. (M) (Top) Image showing
933 the position (dotted line) along which kymographs (bottom) of Emerald-mEps8 and FusionRed-F-tractin
934 were made from time-lapse movies of their dynamics in leader blebs. Scale bar: 2 min (N) Color
935 encoded time-overlay of images of Emerald-F-tractin in a migrating cell. Error is SEM, * $p \leq 0.05$, **
936 $p \leq 0.01$, *** $p \leq 0.001$, **** $p \leq 0.0001$, NS: $p > 0.05$. See also Videos 1-3.

937
938

Figure 2. Eps8 promotes leader bleb-based migration by maintaining actin bundles towards the distal bleb tip.

939
940
941
942
943
944
945
946
947
948
949
950
951
952
953
954
955
956
957
958
959

(A) (Left) Representative blot and (right) quantitation of Western blot analyses of Eps8 and Erk in lysates of A375 (gray), U20S (blue) and A549 (green) cells that were treated with non-targeting siRNAs (non-targeting) or siRNAs targeting human Eps8 to deplete Eps8 (hEps8 siRNA). (B-H) Images and analyses of cells plated on glass and confined under an agar slab. (B) Color encoded time-overlay of confocal images through the central Z-plane of an A375 cell depleted of Eps8 and expressing soluble EGFP. (C, G) Tukey box plots showing (C) quantification of leader bleb area expressed as a % of cell body area for cells treated with non-targeting or Eps8 siRNAs, with or without the additional expression of mouse Eps8 (mEps8 WT). “+” and line denote the mean and median, respectively. (D) Quantitation of the percent of cells that migrate from time-lapse phase contrast movies, treatments as in (C). (E-F) Confocal images through the ventral Z-plane of an A375 cell depleted of Eps8 and expressing Emerald-F-tractin (E) and FusionRed-myosin II regulatory light chain ((F), RLC), boxed area in E shown at right, overlay of (E) and (F) shown at left of (F). (G) Analysis of cortical actin density in A375 cells (see Supplemental Methods) in the cell body from images of phalloidin, treatments as in (C), normalized to the mean value of non-targeting control. (H) Regional analysis of the average fluorescence intensity (H, normalized to maximum) and bundle anisotropy (H’) of FusionRed-F-tractin along leader blebs in A375 cells treated with either non-targeting or human Eps8 siRNAs. Each point represents the average value in a region of interest (ROI) that is 20% of the length of the leader bleb. (I) Western blot analyses of Eps8, myosin II regulatory light chain (MLC), and myosin II regulatory light chain phosphorylated on serine 19 (pMLC (S19) in lysates of A375 cells that were treated with non-targeting siRNAs (non-targeting) or siRNAs targeting human Eps8 to deplete Eps8 (hEps8 siRNA). Error in (A, H) is SEM, * p≤0.05, ** p≤0.01, *** p≤0.001, **** p≤0.0001, NS: p>0.05.

960 **Figure 3. Cortex tension and intracellular pressure are maintained by Eps8.**

961 (A) Schematic representation of the Atomic Force Microscope (AFM) based assay for
962 determining cortex tension and intracellular pressure in A375 cells plated on uncoated glass. “ k_c ”
963 cantilever spring constant, “ d ” cantilever deflection, “ z ” piezo Z displacement (B) (Left) confocal image of
964 the central Z plane or (right) x-y projection of a 3D reconstruction of a Z-stack of a cell expressing EGFP
965 as a volume marker. (C-D) Tukey box plots of cortex tension (C) and intracellular pressure (D)
966 determined from AFM analysis. “+” and line denote the mean and median, respectively. Cells were
967 treated with 50 μ M blebbistatin, non-targeting siRNAs, siRNAs targeting human Eps8 (hEps8) with or
968 without the additional expression of Emerald-tagged mouse Eps8 (mEps8). * $p \leq 0.05$, ** $p \leq 0.01$, ***
969 $p \leq 0.001$, **** $p \leq 0.0001$, NS: $p > 0.05$.

Figure 4. Actin bundling by Eps8 promotes cortex tension and intracellular pressure to drive leader bleb formation.

(A) Schematic representation of wild-type (WT) mouse Eps8 (mEps8) mutant constructs. Top: wild-type Eps8. “*” indicates one part of the split PH domain, “dSH2” indicates degenerate SH2, “capping” indicates domain required for actin capping and which is subject to negative regulation by the Raf/MEK/Erk pathway, “bundling” indicates the domain required for actin bundling. “Δbund” indicates the bundling defective double point mutant L757A/K759A (red bars), “Δcap” indicates the capping defective double point mutant V689D/L693D (red bars), “SATA” indicates double alanine point mutation of Erk phosphorylation sites S624A/T628A (red bars). (B-I) Images and analyses of A375 cells plated on glass and confined under an agar slab. (C, D, G-I) Tukey box plots in which “+” and line denote the mean and median, respectively. (C-D) Quantification of leader bleb area expressed as a % of cell body area for (C) cells treated with non-targeting or Eps8 siRNAs, with or without the additional expression of Emerald-mEps8, Emerald-mEps8Δbund or EGFP human α-actinin or (D) cells over-expressing (OE) Emerald-mEps8, Emerald-mEps8Δbund or EGFP human α-actinin. Data for mEps8 are re-displayed from Figure 2 for comparison. (E) Quantitation of the percent of cells that migrate from time-lapse phase contrast movies, treatments as in (C). (F) Confocal images through the ventral Z-plane of a cell depleted of Eps8 and co-expressing Emerald-mEps8Δbund and either FusionRed-F-tractin (top) or FusionRed-myosin II regulatory light chain (bottom, RLC). (G) Analysis of cortical actin density (see Supplemental Methods) in the cell body from images of phalloidin, treatments as in (D), normalized to the mean value of over-expression of soluble EGFP (EGFP alone). (H-I) Cortex tension (H) and intracellular pressure (I) determined from AFM analysis of cells under the conditions described in (D). * p≤0.05, ** p≤0.01, *** p≤0.001, **** p≤0.0001, NS: p>0.05. See also Video 4.

Figure 5. Eps8 actin capping activity limits leader bleb size by decreasing actin density and mechanical properties in the cell body cortex, and antagonizing actin bundling at the leader bleb tip.

(A-I) Images and analyses of A375 cells plated on glass and confined under an agar slab. **(A)** Color encoded time-overlay of confocal images through the central Z-plane of a cell depleted of Eps8 by siRNAs targeting human Eps8 (hEps8 siRNA) and expressing Emerald-mEps8Δcap (see figure 4A). **(B, C, F, H, I)** Tukey box plots in which “+” and line denote the mean and median, respectively. **(B-C)** Quantification of leader bleb area expressed as a % of cell body area for **(B)** cells treated with hEps8 siRNAs and additionally expressing wild type (WT) Emerald-mEps8 or Emerald-mEps8Δcap or **(C)** cells over-expressing (OE) Emerald-mEps8-WT or Emerald-mEps8Δcap. Data for mEps8 WT are re-displayed from figure 2 for comparison. **(D)** Quantitation of the percent of cells that migrate from time-lapse phase contrast movies, treatments as in **(B)**. **(E)** Confocal images through the ventral Z-plane of cells depleted of Eps8 and co-expressing Emerald-mEps8Δcap and either FusionRed-F-tractin (top) or FusionRed-myosin II regulatory light chain (bottom, RLC). **(F)** Analysis of cortical actin density (see Supplemental Methods) in the cell body from images of phalloidin, treatments as in **(C)**, normalized to the mean value of over-expression of soluble EGFP (EGFP alone). **(G)** Regional analysis of the average fluorescence intensity (G, G', normalized to maximum) Emerald-mEps8 or Emerald-mEps8Δcap (G) or FusionRed-F-tractin (G') and bundle anisotropy (G'') of FusionRed-F-tractin along leader blebs in cells treated with hEps8 siRNA. Each point represents the average value in a region of interest (ROI) that is 20% of the length of the leader bleb. **(H-I)** Cortex tension (H) and intracellular pressure (H) determined from AFM analyses of cells under the conditions described in **(D)**. * p≤0.05, ** p≤0.01, *** p≤0.001, **** p≤0.0001, NS: p>0.05. See also Video 5.

Figure 6. Inhibition of Erk activity perturbs leader bleb-based migration.

(A) Top two panels: Western blot analysis of anti-GFP immunoprecipitates from lysates of A375 cells that were expressing EGFP or Emerald-mEps8 that were or were not treated with 10 μ M U0126 to inhibit Erk. Blot was probed with antibodies specific to phospho-serine and phospho-threonine (pS/T, upper panel) or GFP (upper middle panel). Bottom two panels: Western blot analysis of Erk and Erk phosphorylated on T202/Y204 (pErk) in lysates of untreated A375 that were expressing GFP or Emerald-mEps8 that were or were not treated with 10 μ M U0126. **(B)** Immuno-localization of endogenous Eps8 (green) and phalloidin staining of actin (red) in untreated and U0126 (10 μ M)-treated A375 cells that were non-specifically adhered to poly-L-Lysine coated glass. Arrows: Eps8 localizing to the tips of filopodia. **(C-H)** Images and analysis of A375 cells plated on glass and confined under agarose. **(C)** Time-lapse confocal image series of a cell that was co-expressing FusionRed-F-tractin (top) and EGFP tagged myosin II regulatory light chain (RLC, bottom). Time indicates minutes relative to perfusion with 10 μ M U0126. **(D, F, G, H)** Tukey box plots in which “+” and line denote the mean and median, respectively, treatments as in (A). **(D)** Quantification of leader bleb area expressed as a % of cell body area. **(E)** Quantitation of the percent of cells that migrate from time-lapse phase contrast movies. **(F)** Analysis of cortical actin density (see Supplemental Methods) in the cell body from images of phalloidin, normalized to the mean value of untreated cells. **(G, H)** Cortex tension (G) and intracellular pressure (H) determined from AFM analyses of cells. * $p \leq 0.05$, ** $p \leq 0.01$, *** $p \leq 0.001$, **** $p \leq 0.0001$, NS: $p > 0.05$. See also Video 6.

Figure 7. MEK/Erk-mediated phosphorylation of S624 and T628 coordinates Eps8 capping and bundling activities to mediate leader bleb-based migration.

(A-J) Images and analyses of A375 cells plated on glass and confined under an agar slab. **(A)** Color encoded time-overlay of confocal images through the central Z-plane of a cell depleted of Eps8 by siRNAs targeting human Eps8 (hEps8 siRNA) and expressing Emerald-mEps8 bearing double alanine point mutation of Erk phosphorylation sites S624A/T628A (Emerald-mEps8-SATA). **(B, C, F, I, J)** Tukey box plots in which “+” and line denote the mean and median, respectively. (B-C) Quantification of leader bleb area expressed as a % of cell body area for (B) cells treated with hEps8 siRNAs and additionally expressing wild type (WT) Emerald-mEps8 or Emerald-mEps8-SATA or (C) cells over-expressing (OE) Emerald-mEps8-WT or Emerald-mEps8-SATA. **(D)** Quantitation of the percent of cells that migrate from time-lapse phase contrast movies, treatments as in **(B)**. **(E)** Confocal images through the central Z-plane of cells depleted of Eps8 and co-expressing Emerald-mEps8-SATA and either FusionRed-F-tractin (top) or FusionRed-myosin II regulatory light chain (bottom, RLC). **(F)** Analysis of cortical actin density (see Supplemental Methods) in the cell body from images of phalloidin, treatments as in **(C)**, normalized to the mean value from over-expression of Emerald-mEps8 WT. **(G)** Confocal images through the central Z-plane of cells treated with 10 μ M U0126 and over-expressing either Emerald-mEps8 WT or Emerald-mEps8 Δ bund (see figure 4A) and actin stained with fluorescent phalloidin. **(H)** Quantitation of the percent of cells containing central actin bundles from confocal images of fluorescent phalloidin-stained cells. “F-tractin” indicates over-expression of FusionRed-F-tractin, “UO” indicates treatment with 10 μ M U0126, “mEps8,” “mEps8 Δ cap,” “mEps8 Δ bund,” “mEps8-SATA,” indicate over-expression of EGFP-tagged versions of the respective constructs (see figure 4A). **(I, J)** Cortex tension (I) and intracellular pressure (J) determined from AFM analyses of cells under the conditions described in (C). * $p \leq 0.05$, ** $p \leq 0.01$, *** $p \leq 0.001$, **** $p \leq 0.0001$, NS: $p > 0.05$. See also Video 7.

Figure 8. Erk activity is concentrated in a gradient across leader blebs by a diffusion barrier at the bleb neck.

(A-E, G) A375 cells expressing the EKAREV biosensor in which a CFP-tagged phospho-peptide-binding domain is connected by the EV linker to a YFP-tagged Erk substrate peptide and FRET is obtained when the substrate is phosphorylated by Erk. **(A)** (Left) Confocal image at the ventral Z-plane of the distribution of EKAREV (CFP channel) in a cell plated on fibronectin coated glass. (Right) Pseudocolored ratio image of EKAREV FRET (YFP over CFP emission). **(B)** (Left) Confocal image at the central Z-plane of the distribution of EKAREV (CFP channel) in a cell plated on glass. (Right) Pseudocolored ratio image of EKAREV FRET (magnitude of YFP over CFP emission). **(C)** (Top) Time-lapse confocal image series at the central Z-plane of the distribution of EKAREV (CFP channel) in a cell plated on glass. (Bottom) Pseudocolored ratio image of EKAREV FRET. **(D-H)** Images and analysis of A375 cells cell plated on glass and overlaid with an agar slab. **(D)** (Left) Confocal image at the central Z-plane of the distribution of EKAREV (CFP channel). (Center) Pseudocolored ratio image of EKAREV FRET. (Right) Zoom of the boxed area. **(E)** Regional analysis of the average fluorescence intensity of EKAREV (CFP channel) or the EKAREV FRET (YFP over CFP emission) (normalized to maximum) along leader blebs. Each point represents the average value in a region of interest (ROI) that is 20% of the length of the leader bleb. **(F)** Confocal image at the central Z-plane of the distribution of EGFP tagged Erk, MEK or B-Raf (V600E) in cells which are confined under agarose. **(G)** Quantification of the average ratio of signal in the leader bleb to that in the cell body for (D, F). “Emission ratio” indicates EKAREV FRET signal (YFP over CFP emission), “EKAREV” indicates EKAREV CFP channel, “EGFP alone” indicates soluble EGFP. **(H)** A375 cell expressing soluble mEos2. Time-lapse confocal image series at the central Z-plane. Box indicates the region near the neck of the leader bleb to which a pulse of 405 nm light was applied to locally photo-convert mEos2 from green to red fluorescence. Pseudocolor indicates the magnitude of red fluorescence from mEos2 after photo-conversion. **(I)** Speculative model for Eps8 function during leader bleb-based migration. * $p \leq 0.05$, ** $p \leq 0.01$, *** $p \leq 0.001$, **** $p \leq 0.0001$, NS: $p > 0.05$. See also Videos 8-9.

SUPPLEMENTAL FIGURE LEGENDS

Figure 1-figure supplement 1. Eps8 and ezrin localization. (A) Confocal image of the ventral Z-plane of human melanoma A375 cells spread on fibronectin-coated glass and immunostained for endogenous Eps8 (green) and phalloidin to stain actin (red). (B) (Left) Central Z-plane confocal image of EGFP tagged Ezrin in cells plated on uncoated glass. (Right) time-lapse series of EGFP-Ezrin (green) and rhodamine-dextran (red) used as a negative stain in the culture media to detect the position of the cell membrane. Time (sec) relative to the formation of a bleb. (C, D) Cells confined between uncoated glass and an agar slab, boxed areas shown zoomed to the right. (C) Confocal image of the central Z-plane of Emerald-mEps8 (green) co-expressed with FusionRed-F-tractin (red). (D) Central Z-plane of Emerald-mEps8 (green) and FusionRed-myosin II regulatory light chain (RLC, red) in cells confined between uncoated glass and an agar slab.

Figure 1-figure supplement 2. Detailed view of Eps8 and actin localization. (A) Confocal image of the ventral Z-plane of an A375 cell confined between uncoated glass and an agar slab that was expressing Emerald-mEps8 (green, upper left) and FusionRed-F-tractin to stain actin (red, lower left). Higher magnification views of color-encoded overlay shown at (center) and (right).

Figure 2-figure supplement 1. Myosin II localization is unperturbed in human melanoma A375 cells depleted of and rescued with Eps8. (A-C) Confocal images of A375 cells confined between uncoated glass and an agar slab, magnification is the same in all panels. (Left) Central and (right) ventral Z-plane confocal images of FusionRed-myosin II regulatory light chain (RLC (red)) in cells treated with (A) non-targeting siRNA or (B-C) siRNA directed towards human Eps8 (hEps8 siRNA) with (C) or without (A, B) the additional expression of Emerald-tagged mouse Eps8 (mEps8) and FusionRed-RLC (red).

Figure 2-figure supplement 2. Eps8 is required for leader bleb formation in A549 and U2OS cells. (A) Phase contrast image of an A549 cells (Left) or a U2OS cells (right) plated on uncoated glass coverslip. (B) Color encoded time-overlay of confocal images through the central Z-plane of an A549 cell (left) or a U2OS cell (right) depleted of Eps8 and expressing soluble EGFP and confined between uncoated glass and an agar slab.

Figure 3-figure supplement 1. Actin cortex thickness and cell radii are not significantly affected by depletion of and rescue with wild type Eps8 or its mutants. (A) Example central Z-plane confocal images of a bleb-free region of an A375 cell cortex plated on uncoated glass and stained with Alexa Fluor 568-conjugated Wheat Germ Agglutinin (WGA, green) to mark the position of the cell membrane and Alexa Fluor 647-conjugated phalloidin (Phall, red) to mark the position of the actin cortex for making thickness measurements. (B) Example line-scans of the cell membrane (WGA, green) and actin cortex (phalloidin, red) from (A, white bar) used for determining actin cortex thickness. (C) Average actin cortex thickness determined from confocal images of A375 cells plated on uncoated glass and stained as in (A). (D) Cell radii measurements from phase contrast images of live A375 cells acquired during atomic force microscopy analyses. Error is SD. NS: $p > 0.05$. Conditions are as follows: 50 μ M blebbistatin, non-targeting siRNAs, siRNAs targeting human Eps8 (hEps8) with or without the additional

over-expression (OE) of Emerald-tagged mouse Eps8 (mEps8) variants (“mEps8 Δ cap,” “mEps8 Δ bund,” “mEps8-SATA,” Emerald-tagged versions of the respective constructs (see figure 4A) or 10 μ M U0126.

Figure 4-figure supplement 1. Eps8 bundling activity is not required for myosin II localization to the cortex of A375 cells. (A) Confocal images of A375 cells confined between uncoated glass and an agar slab. (A) Central and (A') ventral Z-plane confocal images of FusionRed-myosin II regulatory light chain (RLC, red) in cells treated with siRNA directed towards human Eps8 (hEps8 siRNA) and additionally expressing Emerald-tagged mouse Eps8 bearing double point mutations L757A/K759A that block its actin bundling activity (green, “mEps8 Δ bund”).

Figure 4-figure supplement 2. Ectopically expressed α -actinin localizes to the leader bleb cortex. (A) Confocal images of A375 cells treated confined between uncoated glass and an agar slab that were treated with siRNA directed towards human Eps8 (hEps8 siRNA) and additionally expressing FusionRed-F-tractin (red) to mark actin filaments and GFP-tagged human α -actinin (green).

Figure 5-figure supplement 1. Eps8 capping activity is not required for myosin II localization to the cortex or leader bleb in A375 cells. (A) Confocal images of A375 cells confined between uncoated glass and an agar slab. (A) central and (A') ventral Z-plane confocal images of FusionRed-myosin II regulatory light chain (RLC, red) in cells treated with siRNA directed towards human Eps8 (hEps8 siRNA) and additionally expressing Emerald-tagged mouse Eps8 bearing double point mutations V689D/L693D that inactivate its actin capping activity (green, “mEps8 Δ cap”).

Figure 6-figure supplement 1. Erk inhibition causes A375 cell flattening. (A) X-Y projections of 3D reconstructions of Z-stacks of paraformaldehyde fixed A375 cells plated on poly-L-Lysine coated glass to mediate non-specific adhesion to the coverslip during immunostaining for endogenous Eps8 (green) and stained with phalloidin to visualize actin (red). (Top) An untreated cell non-specifically adhered poly-L-Lysine coated glass. (Bottom) A cell treated for 90 min with 10 μ M U0126 to inhibit Erk. Z-stacks consisted of 30 confocal slices separated by 0.5 microns. Reconstructions were rendered using “Volume Viewer” in Fiji (<http://fiji.sc/Fiji>).

Figure 7-figure supplement 1. Non-phosphorylatable Eps8 co-localizes with F-actin and not intermediate filaments. (A) Paraformaldehyde fixed A375 cell plated on uncoated glass over-expressing Emerald-tagged mouse Eps8 with the Erk phosphorylation sites mutated (S624A/T628A, Eps8-SATA, green) and stained with phalloidin to visualize actin (red). (B) Live A375 cell confined between uncoated glass and an agar pad and expressing Emerald-mEps8-SATA (green) and FusionRed tagged human vimentin (FusionRed-vimentin) to mark intermediate filaments (red). (A, B) Confocal images of the central (left) or ventral (right) Z-planes. Boxed area shown zoomed at bottom.

Figure 7-figure supplement 2. Inhibition of Eps8 capping activity is not sufficient to maintain leader blebs in the presence of Erk inhibitor. (A) Time-lapse confocal image

1163 series of an A375 cells plated on glass and confined under agarose cell that was treated with
1164 siRNA directed towards human Eps8 (hEps8 siRNA) and additionally expressing Emerald-
1165 tagged mouse Eps8 bearing double point mutations V689D/L693D that inactivate its actin
1166 capping activity (green, "mEps8 Δ cap"). Time indicates minutes relative to perfusion with 10 μ M
1167 U0126 to inhibit Erk.

1168 **Figure 8-figure supplement 1. The Erk inhibitor U0126 reduces EKAREV FRET and A375**
1169 **cell blebbing. (A)** Central Z-plane confocal image series of a live A375 cell plated on uncoated
1170 glass expressing the EKAREV biosensor treated with 10 μ M U0126. Pseudocolor reflects the
1171 magnitude of YFP/CFP ratio FRET signal induced by Erk-mediated phosphorylation of the
1172 biosensor (red = high, blue = low). Time (minutes) relative to perfusion of U0126.

SUPPLEMENTAL TABLE LEGEND

Supplementary File 1. Quantitative and statistical analyses of leader bleb area, cortex tension and intracellular pressure for each condition in A375 cells.

(Sheets 1 - 6) Quantitative and statistical analyses of leader bleb area (Sheets 1 and 2, cortex tension (Sheets 3 and 5, expressed in pN/ μ m) and intracellular pressure (Sheets 4 and 6, expressed in Pa) for human melanoma A375 cells treated with non-targeting siRNA (non-targeting) or depleted of Eps8 using an siRNA specific for human Eps8 (hEps8 siRNA), rescued with or over-expressing (OE) Emerald-tagged wild type mouse Eps8 (mEps8 WT) or the following mutants: mEps8 Δ bund (bundling defective, L757A/K759A), mEps8 Δ cap (capping defective, V689D/L693D) and mEps8 SATA (Erk phosphorylation deficient, S624A/T628A), or EGFP-tagged human α -actinin, or treated with 50 μ M blebbistatin to inhibit myosin II or 10 μ M U0126 to inhibit Mek/Erk. **(Sheets 1, 2)** Cells were confined between uncoated glass and an agar pad, leader bleb area is expressed as percent of cell body area. In **(Sheet 1)**, cells were depleted of Eps8 and rescued with WT and mutants of Eps8, in **(Sheet 2)**, cells were over-expressing WT or mutant Eps8. **(Sheets 3 - 6)** Cells were plated on uncoated glass, and where noted, treated with 50 μ M blebbistatin (5 min) to inhibit myosin II or 10 μ M U0126 (30 min) prior to atomic force microscopy analysis. **(Sheets 3, 5)** Cortex tension (expressed in pN/ μ m) in cells **(Sheet 3)** depleted of and rescued with WT Eps8, or **(Sheet 5)** over-expressing WT Eps8 or mutants. **(Sheets 4, 6)** Intracellular pressure (expressed in Pa) in cells **(Sheet 4)** depleted of and rescued with WT Eps8, or **(Sheet 6)** over-expressing WT Eps8 and mutants.

1193 **SUPPLEMENTAL VIDEO LEGENDS**

1194 **Video 1. Human melanoma A375 cells form a single prominent bleb when confined under**
1195 **an agar pad.**

1196 Comparison of central Z-plane confocal time-lapse movies of Emerald-mEps8 dynamics in A375
1197 cells plated on human plasma fibronectin coated glass (left), uncoated glass (middle) and
1198 confined between uncoated glass and an agar pad (right). Scale bar: 5 μ m, elapsed time in
1199 seconds shown.

1200 **Video 2. Human melanoma A375 cells migrate in the direction of a “leader bleb.”**

1201 Central Z-plane confocal time-lapse movie of Emerald-F-tractin showing actin dynamics during
1202 “leader bleb” based migration of an A375 cell confined between uncoated glass and an agar
1203 pad. Scale bar: 5 μ m, elapsed time in minutes shown.

1204 **Video 3. Eps8 and actin flow towards the bleb neck in leader blebs.**

1205 Ventral Z-plane confocal time-lapse movie of Emerald-mEps8 (green) and FusionRed-F-tractin
1206 (red) dynamics showing their coordinated flow towards the bleb neck in an A375 cell confined
1207 between uncoated glass and an agar pad. Scale bar: 5 μ m, elapsed time in seconds shown.

1208 **Video 4. Formation of large leader blebs requires actin bundling by Eps8.**

1209 Central Z-plane confocal time-lapse movie showing Emerald-Eps8 dbund (L757A/K759A
1210 mutations in mouse Eps8 that block its bundling activity) dynamics and small blebs in an A375
1211 cell that has been depleted of Eps8 by siRNA and confined between uncoated glass and an
1212 agar pad. Scale bar: 5 μ m, elapsed time in seconds shown.

1213 **Video 5. Actin capping by Eps8 limits leader bleb size.**

1214 Ventral Z-plane confocal time-lapse movie showing Emerald-Eps8 dcap (V689D/L693D
1215 mutations in mouse Eps8 that block its actin capping activity) dynamics and large leader bleb
1216 formation in an A375 cell that has been depleted of Eps8 by siRNA and confined between
1217 uncoated glass and an agar pad. Scale bar: 5 μ m, elapsed time in minutes shown.

1218 **Video 6. MEK/Erk activity regulates the organization of the actin cortex and is required to**
1219 **form large leader blebs.**

1220 Ventral Z-plane confocal time-lapse movie showing actin (FusionRed-F-tractin, red) and myosin
1221 II (EGFP-myosin II regulatory light chain, RLC, green) dynamics and leader bleb retraction in an
1222 A375 cell confined between uncoated glass and an agar pad. When the word “U0126” appears,
1223 10 μ M U0126 was perfused into the media to inhibit MEK/Erk. Scale bar: 5 μ m, elapsed time in
1224 minutes shown.

1225 **Video 7. Erk phosphorylation of Eps8 is necessary for large leader bleb formation.**

1226 Ventral Z-plane confocal time-lapse movie showing Emerald-Eps8 SATA (S624A/T628A
1227 mutations in mouse Eps8 that block its ability to be phosphorylated by Erk) dynamics and small

1228 blebs in an A375 cell that has been depleted of Eps8 by siRNA and confined between uncoated
1229 glass and an agar pad. Scale bar: 5 μ m, elapsed time in seconds shown.

1230 **Video 8. The EKAREV biosensor reveals concentrated Erk kinase activity within large**
1231 **leader blebs.**

1232 Comparison of central Z-plane confocal time-lapse movies of Erk kinase activity in A375 cells
1233 plated on human plasma fibronectin coated glass (left), uncoated glass (middle) and confined
1234 between uncoated glass and an agar pad (right). Cells were expressing the EKAREV Erk
1235 activity biosensor. Pseudocolor reflects the magnitude of YFP/CFP ratio FRET signal induced
1236 by Erk-mediated phosphorylation of the biosensor (red = high, blue = low). Scale bar: 5 μ m,
1237 elapsed time in seconds shown.

1238 **Video 9. The bleb neck restricts the diffusion of photo-converted mEos2 between large**
1239 **leader blebs and the cell body.**

1240 Central Z-plane confocal time-lapse movie of freely diffusing mEos2 before and after activation
1241 with a 0.5 sec pulse of 405 nm laser light within a defined region (box) of a leader bleb showing
1242 slow diffusion between a large leader bleb and the cell body. Pseudocolor reflects the
1243 magnitude of red fluorescence from mEos2 after photo-conversion (red = high, blue = low).
1244 Scale bar: 5 μ m, elapsed time in seconds shown.

Figure 1.

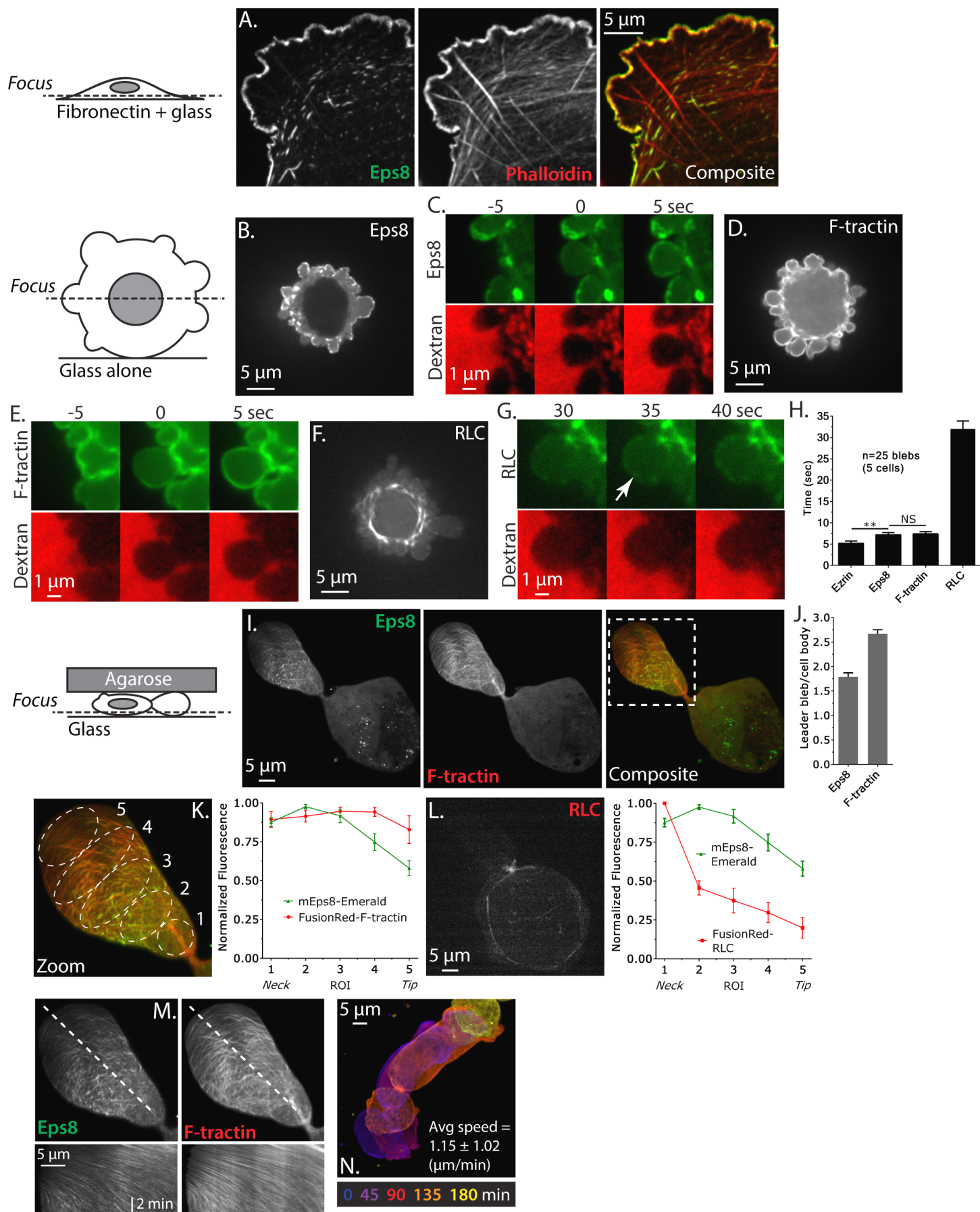


Figure 2.

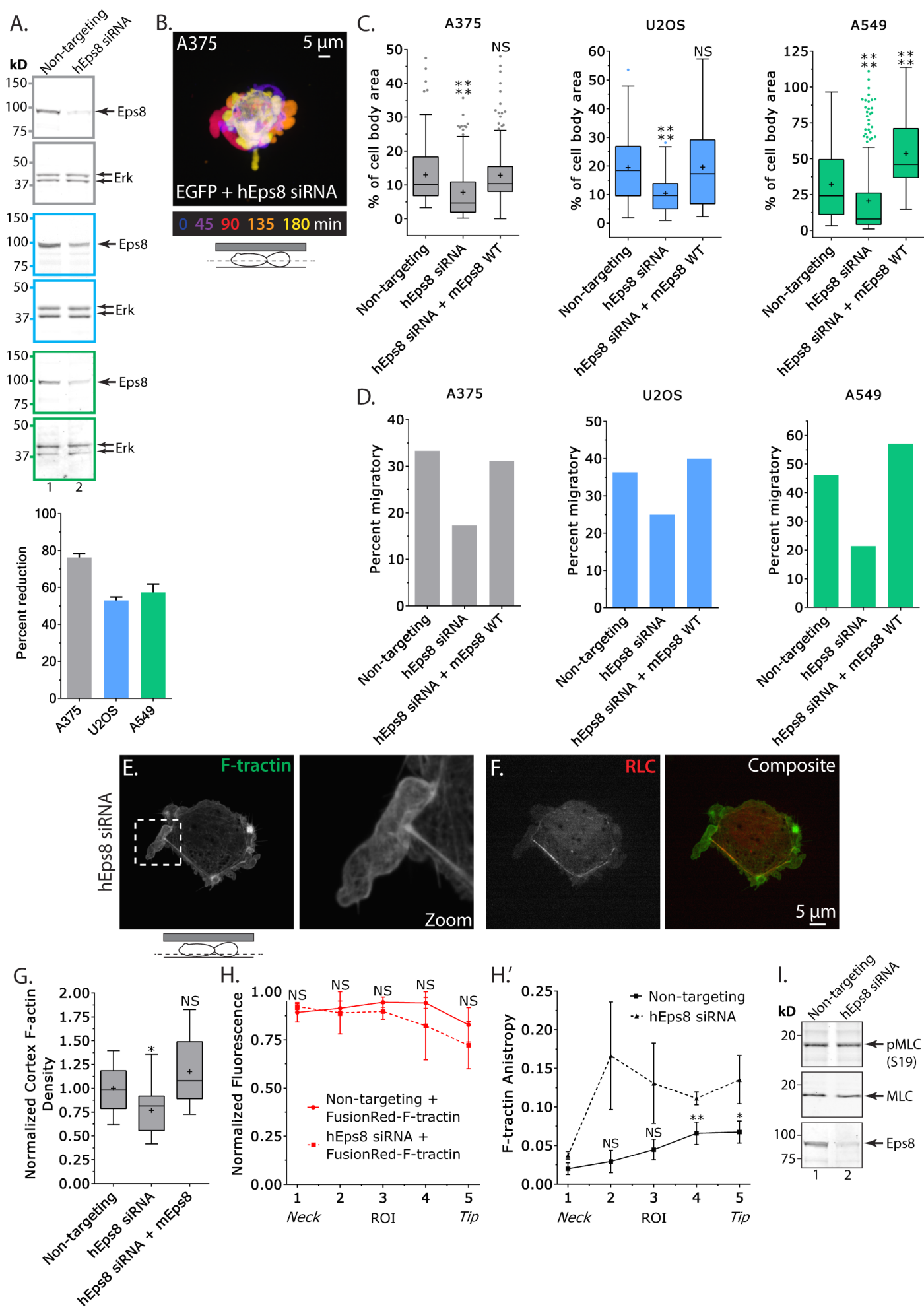


Figure 3.

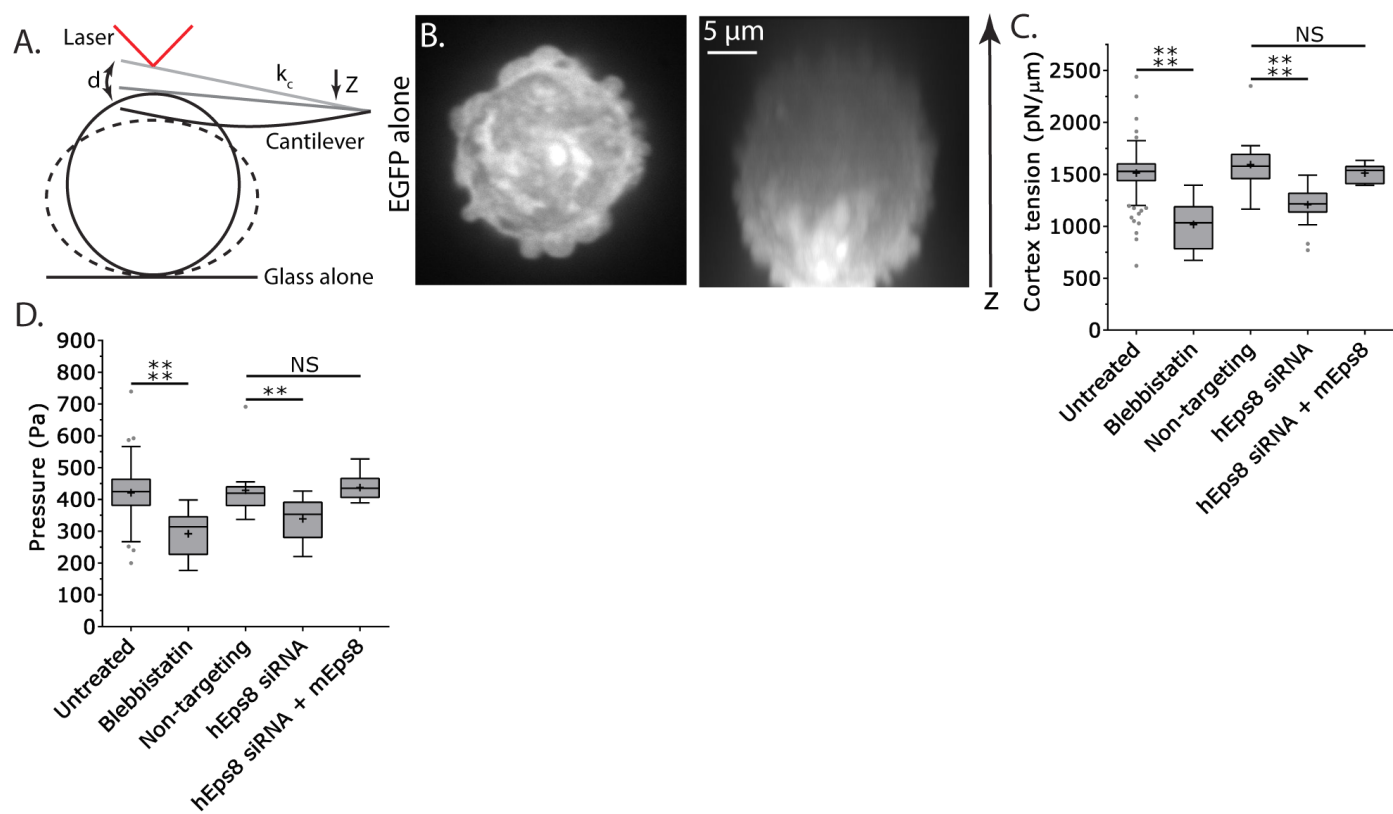


Figure 4.

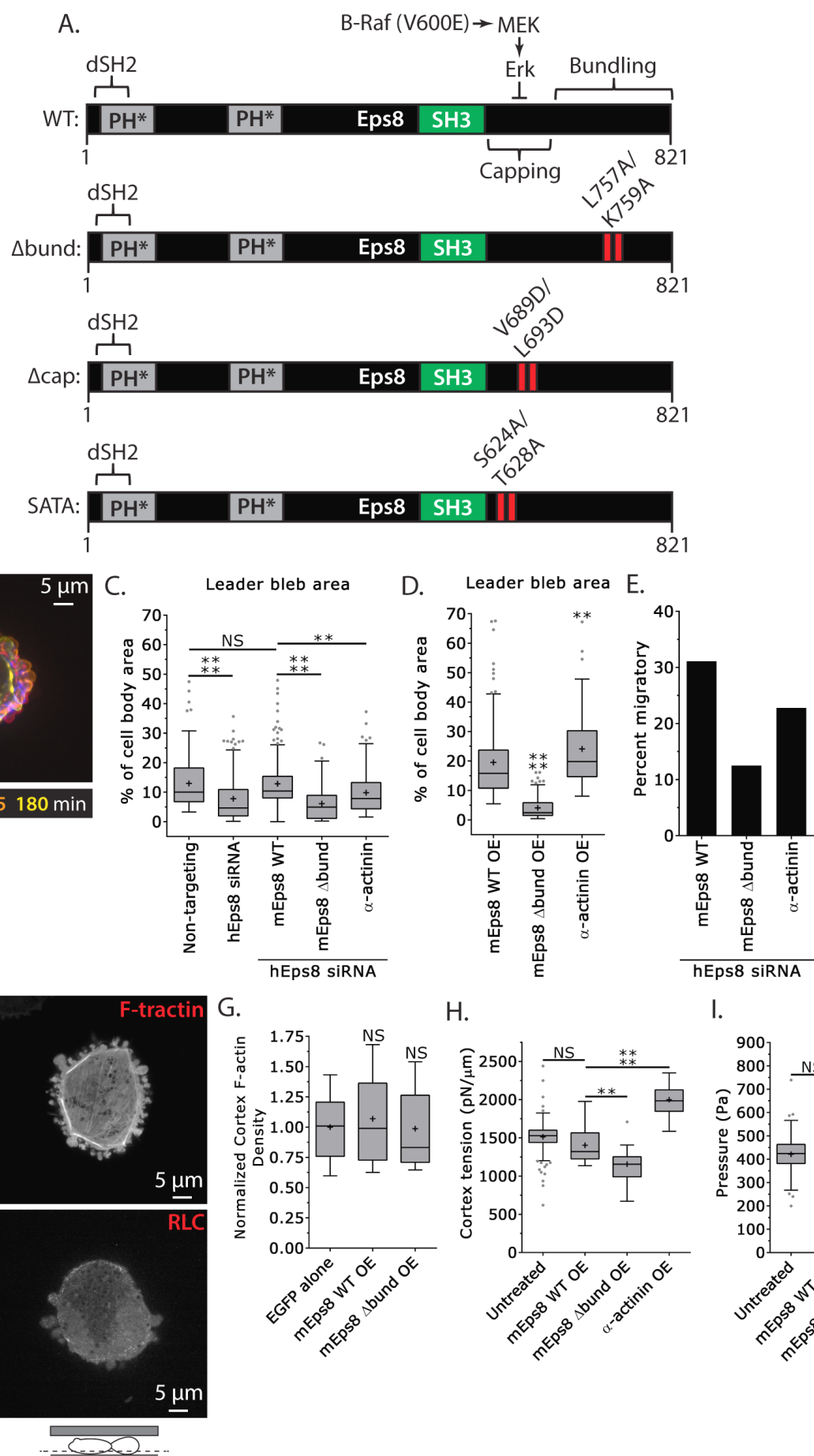


Figure 5.

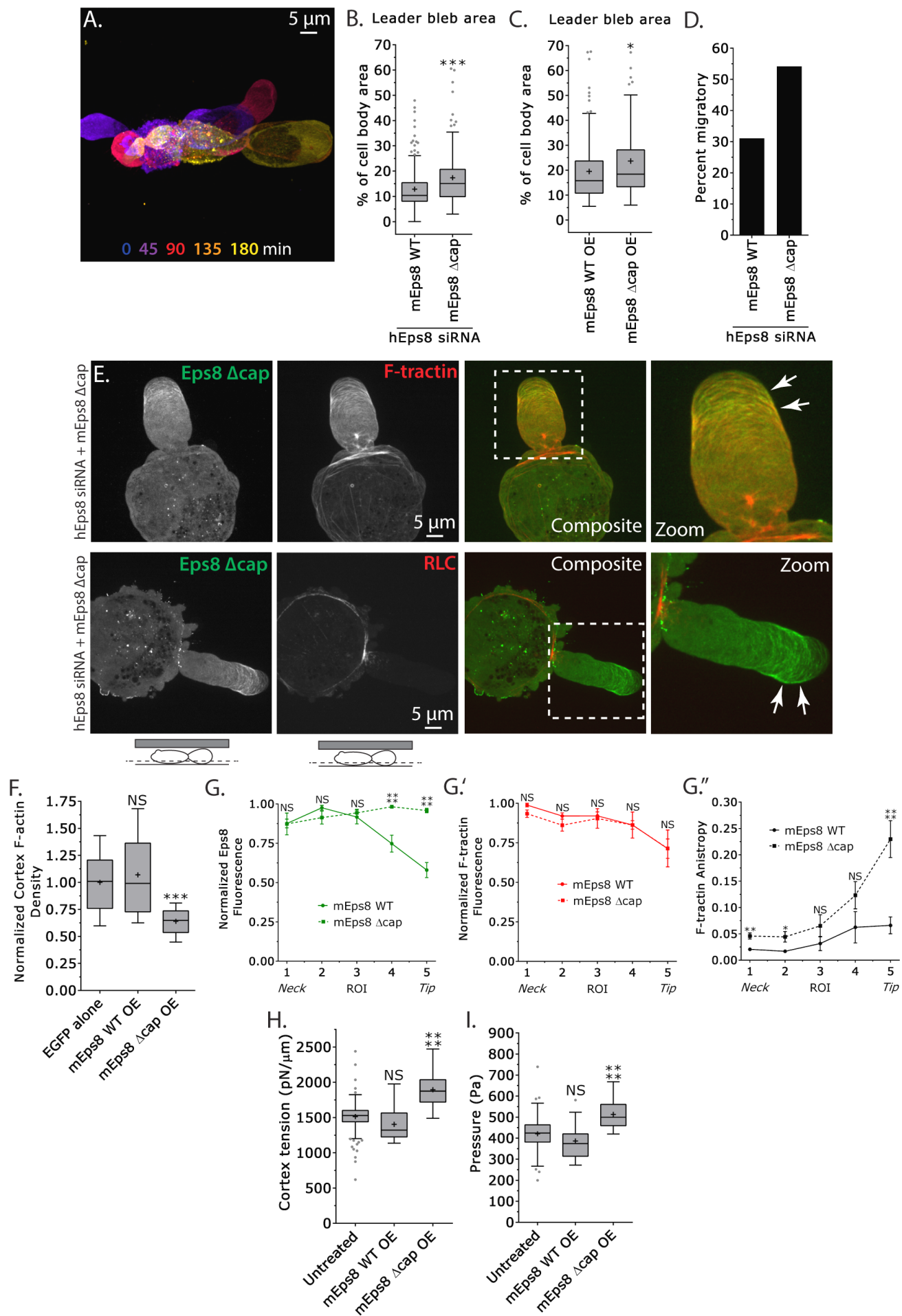


Figure 6.

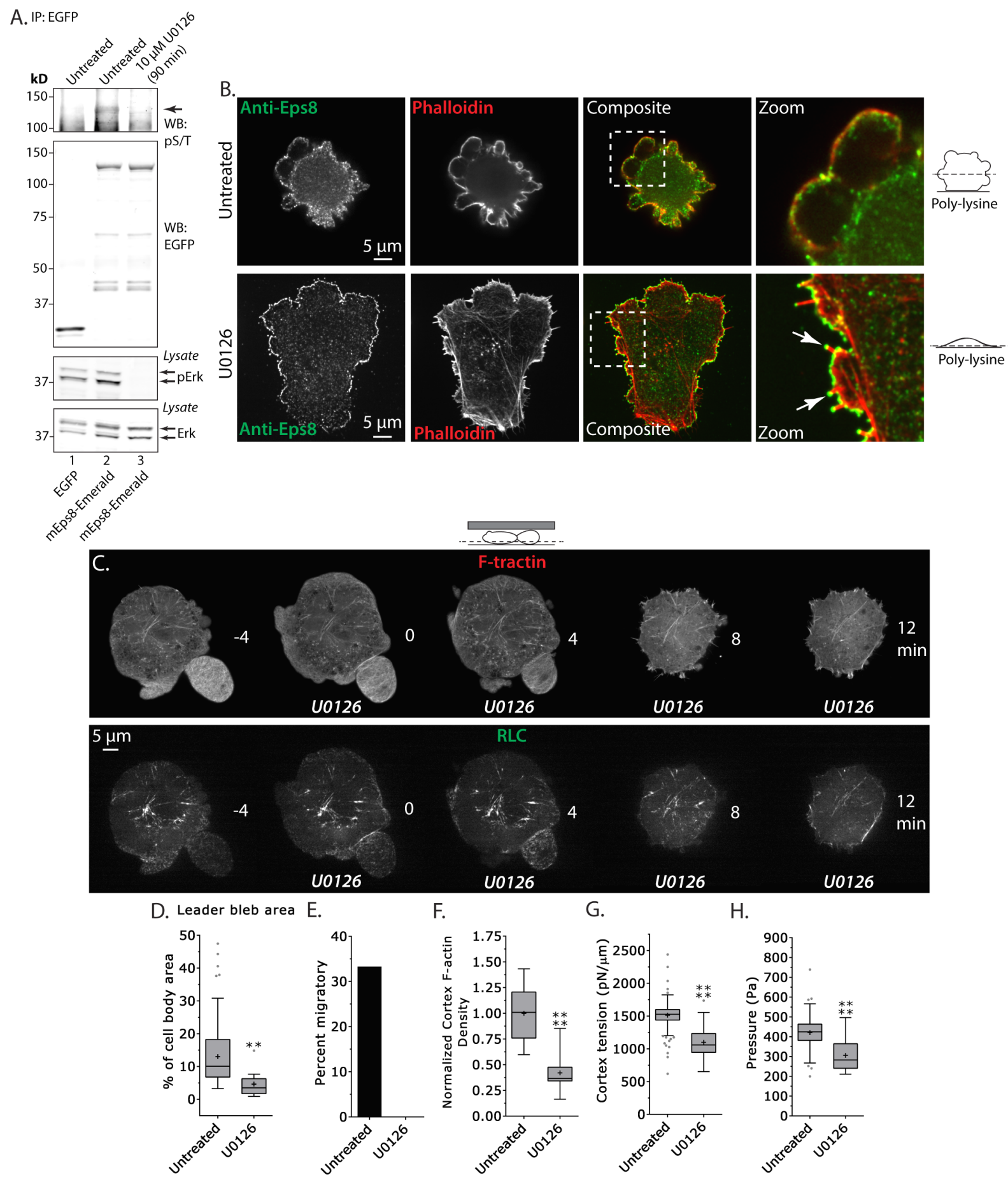


Figure 7.

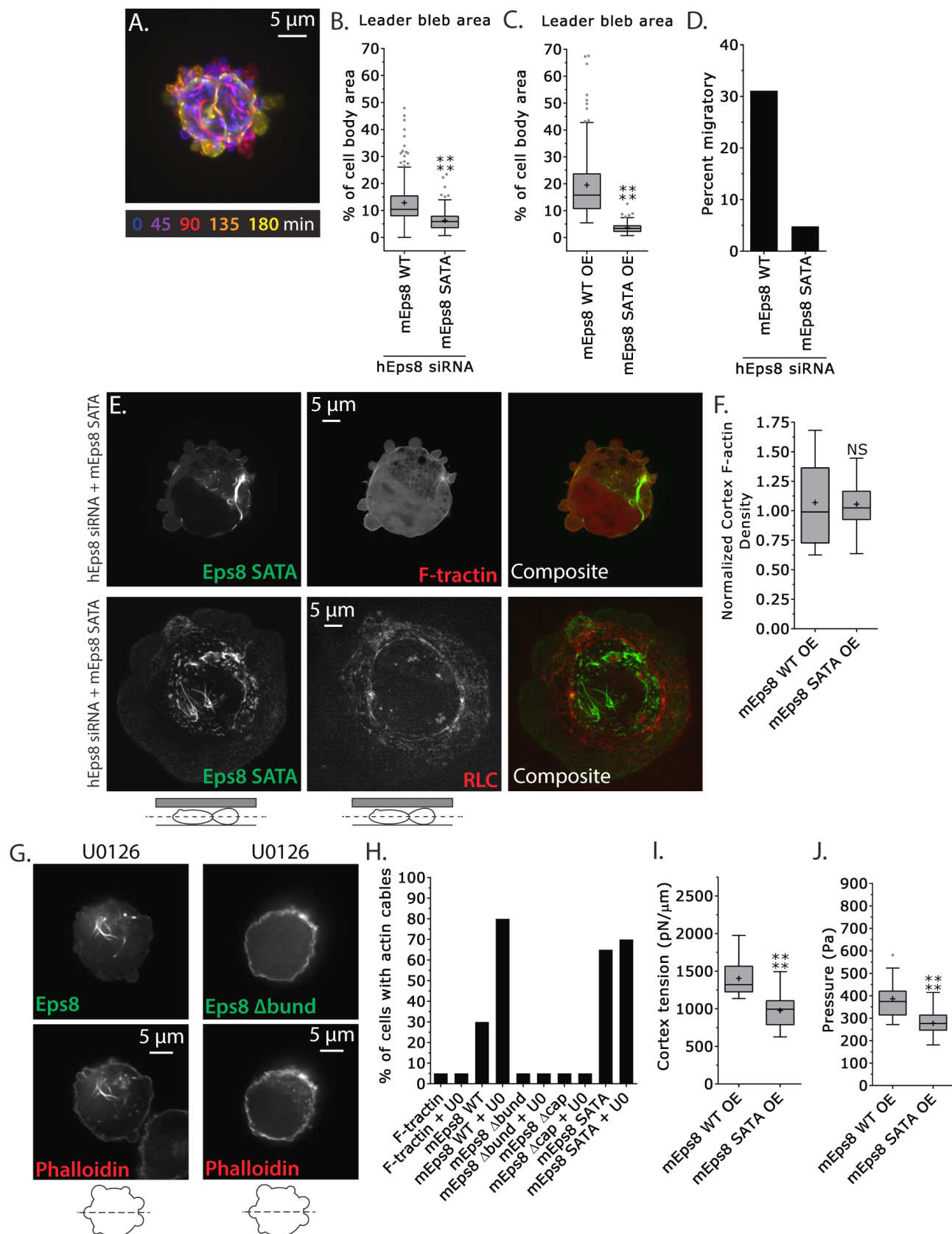


Figure 8.

